

SKIN INFLAMMATION

Psychological stress increases skin infection through the action of TGF β to suppress immune-acting fibroblasts

Hung Chan¹, Fengwu Li¹, Tatsuya Dokoshi¹, Kellen J. Cavagnero¹, Qing Li², Yang Chen¹, Carlos Aguilera¹, Teruaki Nakatsuji¹, Edward Liu¹, Aaryan Indra¹, Daping Yang³, Ottaviani Valentina⁴, Tomofumi Numata¹, Brittany Crown¹, Henry Li¹, Kevin J. Williams⁵, Isaac M. Chiu⁶, Steven J. Bensinger⁷, WanJun Chen⁴, Richard L. Gallo^{1*}

Copyright © 2025 The Authors, some rights reserved; exclusive licensee American Association for the Advancement of Science. No claim to original U.S. Government Works

Infections after psychological stress are a major health care problem. Single-cell transcriptomics and lipidomic profiling in a mouse model of stress show that dermal fibroblasts undergoing adipogenesis have defective responses to *Staphylococcus aureus* skin infection. Adrenalectomy or adrenergic inhibition restores the fibroblast adipogenic response to *S. aureus* and enables mice to effectively resist infection during stress. Increased susceptibility to *S. aureus* from stress is attributed to suppression of the antimicrobial peptide cathelicidin (*Camp*) because adrenaline directly inhibits *Camp* production by fibroblasts, and mice lacking *Camp* in fibroblasts do not increase infection after stress. Transforming growth factor β (TGF β) is induced by stress and adrenergic signaling, and inhibition of TGF β or deletion of the TGF β receptor on fibroblasts increases *Camp* expression and restores protection against infection. Together, these data show that stress initiates a brain-skin axis mediated by TGF β that impairs the immune defense function of dermal fibroblasts to produce the *Camp* antimicrobial peptide.

INTRODUCTION

Psychological stress is a major risk factor that is associated with exacerbation of bacterial infections (1, 2). Stress induces activation of both the hypothalamic-pituitary-adrenal (HPA) axis and the sympathetic nervous system (SNS) (3). Activation of these systems triggers the discharge of catecholamines, including adrenaline from the adrenal medulla and noradrenaline from sympathetic nerve endings in peripheral organs. Activation of the HPA axis also results in production of glucocorticoids by the adrenal cortex (4, 5). Prior studies have generally focused on the responses of classical immunocytes to glucocorticoids to explain the increased susceptibility to infection observed after psychological stress (6–8). However, there is still limited consensus regarding how stress modulates host defense events that are critical to the phenotypes observed. For example, adrenaline reduces major histocompatibility complex (MHC) II expression on various cells, including astrocytes, Langerhans cells, and suppressor T cells. Adrenergic signaling influences trafficking by T cells, as well as cytokine production and proliferation of CD8 $^+$ T cells in chronic viral infection and antitumor immunity (9). Given the complex observations that associate stress with immune suppression, the mechanisms by which psychological stress enhances susceptibility to bacterial infections have remained elusive.

An important mechanism for resistance to skin infection by *Staphylococcus aureus* (SA) is the production of antimicrobial peptides

(AMPs) (10). In particular, the AMP cathelicidin (*Camp*) contributes to host defense through direct killing of SA and indirect actions to amplify inflammatory cell recruitment (10). Although the expression of *Camp* in neutrophils is important to the function of this cell type, several other cell types also express this AMP, including dermal fibroblasts that express *Camp* during preadipocyte differentiation in a process known as reactive adipogenesis (11). The presence of *Camp* in fibroblasts at this stage plays a vital role in constraining the spread of bacteria at barrier tissues (11–13).

In this study, our objective was to gain further insight into the causes of immune dysfunction from psychological stress by conducting an unbiased analysis of the early host defense response to SA in mice. Unexpectedly, we observed that stress reduced the capacity of dermal fibroblasts to differentiate into adipocytes and express *Camp*. This defect in host immunity was driven by transforming growth factor β (TGF β), a signaling system not previously associated with psychological stress. We therefore provide insight into how fibroblasts serve as a relay between brain-derived stress signals and immunosuppression in the skin. Our findings underscore the roles of TGF β and dermal fibroblasts as potential therapeutic targets for mitigating invasive bacterial infections associated with psychological stress.

RESULTS

Psychological stress increases susceptibility to *S. aureus* skin infection

To better understand the changes in host defense that occur after stress, we developed a psychological stress model consisting of transient daily restraint followed by intradermal challenge with SA (Fig. 1A). Compared with littermate controls, intermittent psychological stress for 3 hours per day over 3 days resulted in a large increase in infection by a methicillin-resistant strain of SA (USA300 lac) (14–16) as seen by larger skin lesions and increased colony-forming units (CFU) of SA (Fig. 1, B to D, and fig. S1A). This stress model also increased circulating

¹Department of Dermatology, University of California, San Diego, La Jolla, CA, USA.

²Dermatology Hospital, Southern Medical University, Guangzhou, China. ³Institute of Neuroscience, Center for Excellence in Brain Science and Intelligence Technology, Chinese Academy of Sciences, Shanghai 200031, China. ⁴Mucosal Immunology Section, National Institute of Dental and Craniofacial Research, National Institutes of Health, Bethesda, MD 20892, USA. ⁵Department of Biological Chemistry and UCLA Lipidomics Lab, UCLA, Los Angeles, CA, USA. ⁶Department of Immunology, Harvard Medical School, Boston, MA, USA. ⁷Department of Microbiology, Immunology, and Molecular Genetics, UCLA Lipidomics Lab and Department of Molecular and Medical Pharmacology, UCLA, Los Angeles, CA, USA.

*Corresponding author. Email: rgallo@ucsd.edu

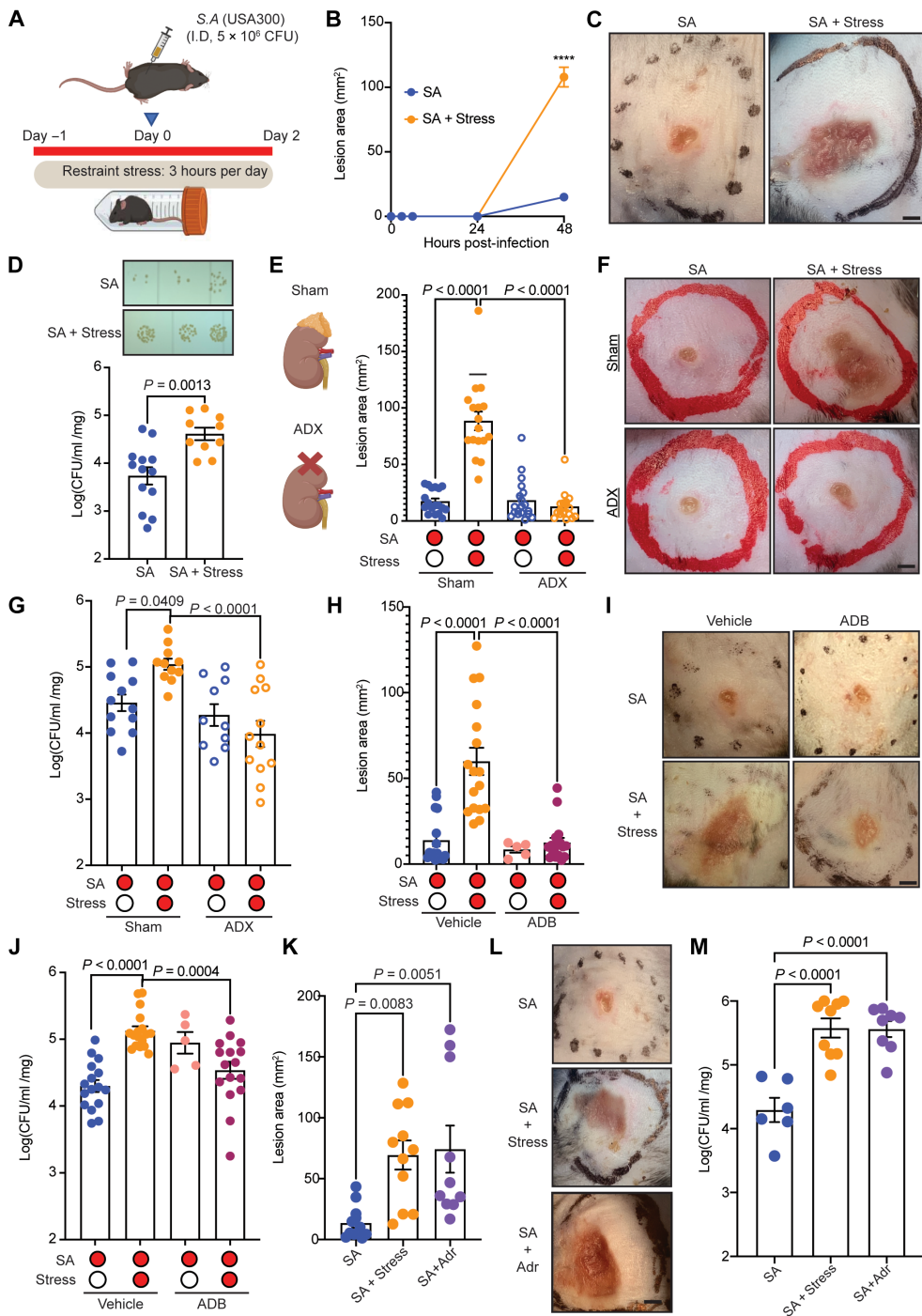


Fig. 1. Psychological stress exacerbates skin infection by S. aureus. (A) Schematic of the experimental stress model by restraint and SA infection. SA was injected immediately before restraint on day 0. (B) SA lesion size was measured at different time points after injection in the absence or presence of psychological stress ($n = 22$ or 23 lesions from 11 or 12 mice for each condition at day 2). **** $P < 0.0001$. (C) Representative photograph of lesions from day 2 after SA injection. Scale bar, 1.5 mm. (D) Image of SA colony growth on agar and quantification of CFU/ml per mg of skin tissue ($n = 10$ to 13 lesions for each condition). (E) Illustration of surgical ADX. Measurements of SA lesion size on day 2 after SA injection and 9 days after sham operation or ADX mice ($n = 17$ to 19 lesions from 9 or 10 mice for each condition). (F) Representative photograph of skin lesions from sham-operated mice or ADX mice 2 days after SA infection. Scale bar, 1.5 mm. (G) SA CFU in skin tissue at day 2 from sham-operated mice or ADX mice in the absence or presence of psychological stress ($n = 10$ to 12 lesions for each condition). (H) Lesion size of SA-infected mice with or without psychological stress after pretreatment with adrenergic receptor blockers (ADB) or vehicle in ($n = 5$ to 17 lesions from three to nine mice for each condition). (I) Representative photograph of lesions from (H). Scale bar, 1.5 mm. (J) SA CFU in skin tissue from experiments shown in (H) ($n = 5$ to 17 lesions from three to nine mice for each condition). (K) Comparison of 2-day SA lesion size after psychological stress or intradermal injection of adrenaline (Adr) (1.6 mg/kg daily) starting from day -1 to day 2. ($n = 10$ to 12 lesions from five or six mice). (L) Representative photograph of lesions from (K). Scale bar, 1.5 mm. (M) SA CFU in skin tissue from experiments shown in (K) ($n = 6$ to 9 lesions for each condition). Results in all panels are represented as means \pm SEM from two or more independent experiments. Significance was calculated using a one-way ANOVA (three or more group comparisons).

adrenaline, noradrenaline, and corticosterone (fig. S1B) and promoted weight loss (fig. S1C).

To determine whether the increase in skin infection by SA was neuronally mediated and not influenced by the topical effects from physical restraint, we next evaluated the response to disruption of the HPA axis. Surgical adrenalectomy (ADX) successfully reduced the increase in infection caused by restraint stress compared with that in mock-surgical controls (Fig. 1, E to G). ADX also eliminated the increase in adrenaline, noradrenaline, and corticosterone and inhibited weight loss caused by stress (fig. S1, D and E). Adrenergic signaling was specifically involved in this axis given that the use of a chemical adrenergic blockade by combining a phenoxybenzamine (α -adrenergic inhibitor) and propranolol (β -adrenergic inhibitor) alleviated the increase in lesion size and SA CFU in mice caused by restraint stress (Fig. 1, H to J). Furthermore, direct administration of adrenaline to mice every day before and after the challenge with SA resulted in an increase in SA infection and loss of weight similar to that seen from psychological stress (Fig. 1, K to M, and fig. S1F). We also found that chemical sympathectomy by pretreatment of mice with 6-hydroxy dopamine (6-OHDA)—a neurotoxin that ablates sympathetic and catecholaminergic, including dopaminergic and noradrenergic, neurons (17, 18)—reduced noradrenaline levels and blocked the stress-induced exacerbation of SA infection (fig. S2, A to E). Therefore, both the HPA axis and sympathetic nerves appeared to be involved in the stress-induced exacerbation of deep skin infection by SA.

The observations described here are consistent with prior studies finding that stress increases susceptibility to infectious agents (19, 20), and this system demonstrates that a deep dermal SA infection of the skin is increased in mice after psychological stress. This model recapitulates the common human disease of cellulitis and provides an experimental approach to subsequently perform an unbiased analysis of the mechanisms by which stress adversely affects skin immune defense.

Acute stress suppresses the host defense response of dermal fibroblasts to SA

We next conducted a bulk transcriptional analysis of mouse skin to understand the local innate host defense response to SA after psychological stress. Principal components analysis (PCA) revealed a distinct skin transcriptomic response to stress and SA that was largely restored by ADX (Fig. 2, A and B). Comparative analysis between SA with stress and SA alone showed that stress was associated with the down-regulation of genes involved in lipid metabolism (*Plin1*, *Thrsp*, and *Gpd1*) and influenced the expression of fibroblast-associated genes (*Igfbp5*, *Fn1*, and *Col5a1*) (Fig. 2C). Gene set enrichment analysis (GSEA) also showed that stress resulted in the down-regulation of genes associated with adipogenesis in the dermis and that this was restored by ADX (Fig. 2D).

Consistent with the decrease in gene expression associated with adipogenesis, histologic examination of skin after stress, or after adrenaline administration, revealed a decrease in the subcutaneous adipose layer and a decrease in lipid staining in the dermis after stress or adrenaline (Fig. 2, E to H). This decrease in dermal fat during stress contrasts with the increase in adipose seen after SA infection of normal skin.

The effects of stress were also tested in alternative models of SA infection by epicutaneous application or injection into the hindpaw (fig. S3). Epicutaneous SA and stress resulted in increased scaling and a thinner epidermis (fig. S3, A and B). Stress during SA injection

into the hindpaw resulted in increased inflammation and epidermal thickening (fig. S3, C and D). However, no significant increase in SA survival was observed after stress in these models (fig. S3, E and F). This response is consistent with the lesser potential for a deep dermal adipogenic response when bacteria are present on the surface or in skin that has minimal dermal fat.

To better understand the effect of stress and SA infection on adipogenesis in back skin after SA infection, we next conducted a lipidomic analysis and targeted quantitative polymerase chain reaction (qPCR) of genes associated with adipogenesis. PCA showed a distinct difference in lipids after stress and SA infection (Fig. 2, I to K), with a change in principal component 1 (PC1) reflecting changes driven by SA infection and PC2 reflecting changes to the lipidome induced by stress (Fig. 2I). Several lipids associated with adipocyte differentiation were decreased by stress and SA infection, including phosphatidylinositol, phosphatidylserine, and phosphatidylcholine (fig. S4, A to O). Although only a small decrease in triglycerides was seen (Fig. 2J), free fatty acids increased, suggesting lipolysis (Fig. 2K). The qPCR evaluation of mRNA for *Pparg2*, a factor important for adipogenesis, was also suppressed by stress at 3 and 48 hours after SA infection (fig. S4P). The qPCR evaluation of mRNA for *Pparg1* and *Pparg2* in response to ADX provided further evidence that adrenergic signaling mediates the inhibition of SA-induced reactive adipogenesis in the dermis (fig. S4, Q to T). These results are consistent with the findings from RNA sequencing (RNA-seq) and histology showing the induction of adipogenesis by SA infection and the inhibition of adipogenesis induced during stress.

Next, single-cell RNA sequencing (scRNA-seq) was conducted to enable a detailed evaluation of the cellular transcriptional response to SA during psychological stress. Using standard Seurat integration methods, we confirmed that batch effects were minimal (fig. S5A). Unbiased clustering with Seurat canonical correlation analysis visualized 27 cell clusters by t-distributed stochastic neighbor embedding (t-SNE) (Fig. 3A). Eight main cell types were delineated from the skin, including fibroblast, myocyte, adipocyte, lymphoid, keratinocyte, endothelial, myeloid, and melanocyte (related marker genes are shown in Fig. 3B). During SA infection, stress strongly suppressed the relative proportion of fibroblasts and led to a relative increase in proportions of myeloid, lymphoid, and keratinocytes (fig. S5B). This was accompanied by distinct patterns of adrenergic receptor expression on several cell types (fig. S5C). Also, stress altered cell subpopulations' distribution and heterogeneity during SA infection (fig. S5, D to L). Specifically, stress increased the proportion of basal keratinocytes (KC2s; *Krt24*⁺; *Lgr5*⁺) (fig. S5, D to F) as well as neutrophils and dendritic cells (fig. S5, G to I) and $\gamma\delta$ T cells (fig. S5, J to L) in the skin. This increase in immune cells correlates with findings from gene set variation analysis (GSVA) of all cells that showed enrichment in pathways related to AMPs, including “metal sequestration by antimicrobial proteins” and “AMPs” in mice with stress and SA infection (Fig. 3C). However, among all clusters from scRNA-seq data, fibroblasts had 10-fold more differentially expressed genes with stress (5644 genes) (Fig. 3D). Furthermore, specific Gene Ontology (GO) and Reactome Pathway enrichment analysis of fibroblasts revealed that stress resulted in the down-regulation of pathways associated with defense response, fat cell differentiation, and cholesterol biosynthesis (Fig. 3E).

On the basis of these observations that stress decreases the proportion of fibroblasts and inhibits the defense response and fat cell differentiation, we next evaluated the expression of several AMPs,

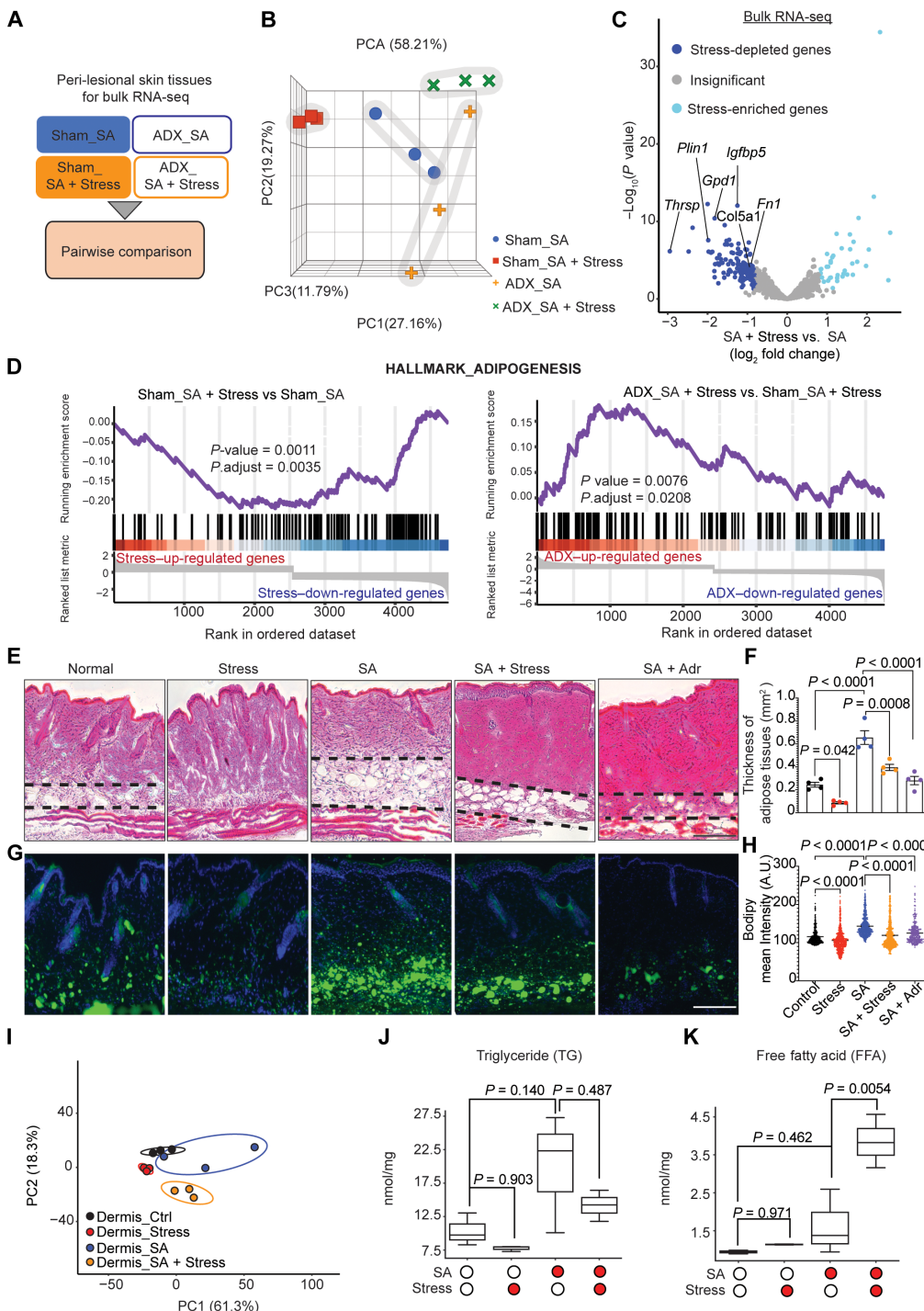


Fig. 2. The suppression of lipid-related host defense mechanisms is linked to the exacerbation of SA infection triggered by psychological stress. (A) Bulk RNA-seq workflow for mouse skin 2 days after SA infection, sham operation, or ADX with or without stress. (B) PCA of the normalized bulk RNA-seq data for (A) ($n = 3$ for each condition). (C) Volcano plot of differentially expressed genes in peri-lesional skin biopsies from sham-operated mice infected with SA alone versus SA-infected controls with stress. (D) Pairwise comparison of GSEA using the Hallmark adipogenesis pathway from bulk RNA-seq data. The comparisons include Sham_SA + stress versus Sham_SA and ADX_SA + stress versus ADX_SA + stress. (E) Histological images of hematoxylin and eosin (H&E) staining of skin samples collected 2 days after SA infection and stress or Adr administration. Adipose tissues are marked with dashed lines (images are representative of $n = 6$ per group). Scale bar, 300 μm . (F) Quantification of adipose tissue thickness shown in (E) ($n = 4$ per group). (G) Bodipy staining of lipid in skin samples collected 2 days after SA infection and stress or Adr administration. Nuclei were stained by DAPI (blue). (H) Quantification of the mean intensity of lipid droplets in (G) ($n = 333$ for control; $n = 685$ for stress; $n = 623$ for SA; $n = 713$ for SA with stress; $n = 361$ for SA with Adr administration). (I) PCA of lipidomic data from dermises of SA-infected mice or vehicle-injected mice in the absence or presence of psychological stress ($n = 3$ for each condition). The percentage of total variance explained by individual principal components (PC1 and PC2) is indicated. (J) Box plot of triglyceride abundance in tissues from (I). (K) Box plot of free fatty acid in tissues from (I). Significance was calculated using a one-way ANOVA (three or more group comparisons). A.U., arbitrary unit.

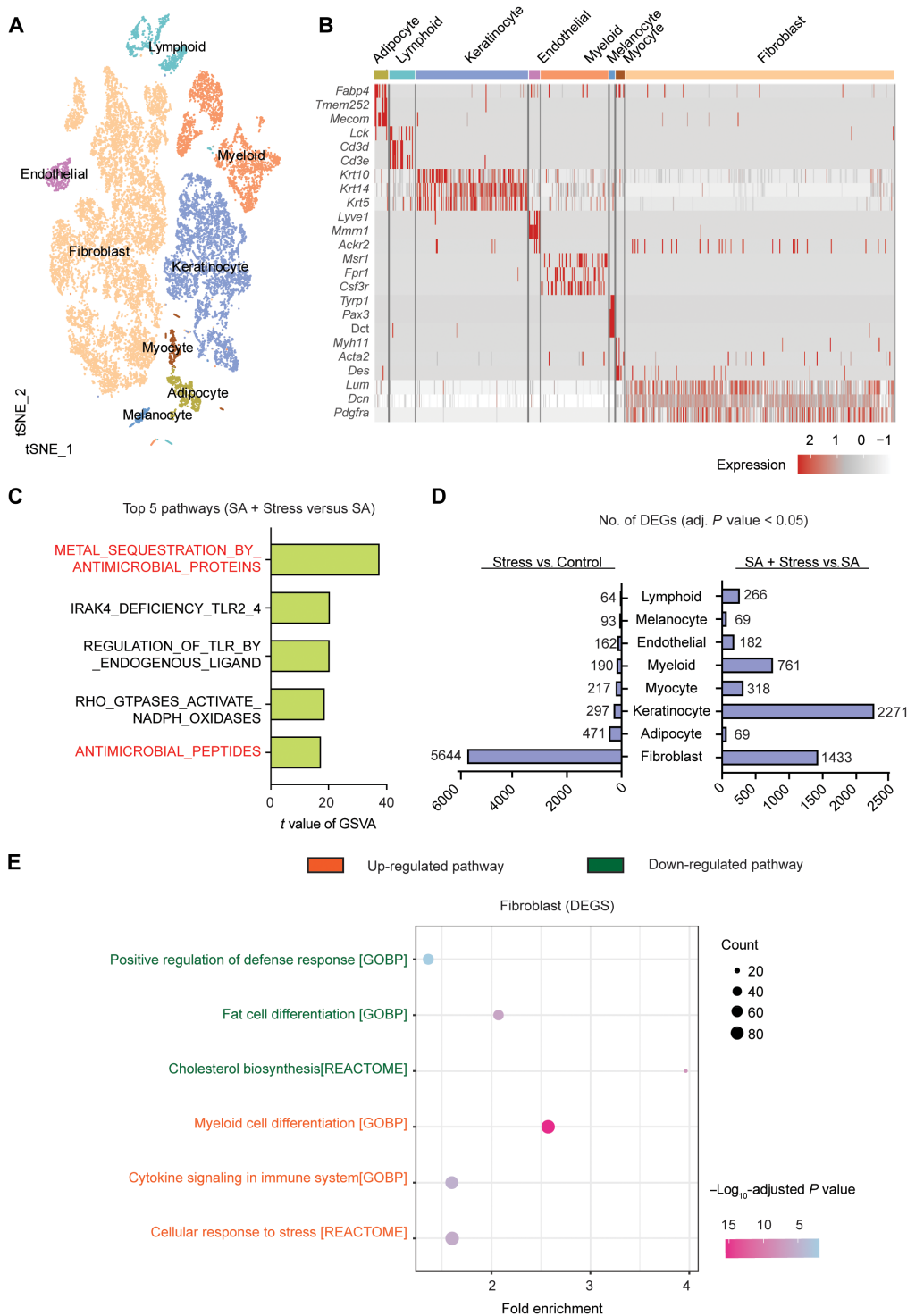


Fig. 3. Psychological stress alters fibroblast gene expression. (A) t-SNE plot of all high-quality cells profiled from pooled dorsal mouse skin 2 days after SA infection and mock infections with or without restraint stress ($n = 3$ animals per condition). A post-quality control analysis identified 5969 cells from mock-infected skin, 5201 cells from mock-infected skin with stress, 3678 cells from SA-infected skin, and 1112 cells from SA-infected skin with stress. (B) Heatmap of the canonical and curated marker genes for major cell lineages. (C) Bar plot demonstrating top five pathways enriched in SA with stress versus SA by GSVA. t values were calculated by limma regression. (D) Number of differentially expressed genes (DEGs) in each cell type in stressed and control skin with or without SA infection (Poisson test, adjusted P value of < 0.05). (E) Illustration representing the number of genes that were either up-regulated or down-regulated in fibroblasts under stress conditions compared with the control group. Enrichment analysis (P value < 0.05 and fold change > 0.25) was conducted for GO biological processes and pathways in the Reactome pathway database, focusing on the genes that exhibited up-regulation or down-regulation in fibroblasts.

including the AMP gene *Camp*. A qPCR approach was used for this gene because *Camp* mRNA is not well detected by scRNA-seq (21). *Camp* is essential for resistance to SA infection and is expressed by fibroblasts undergoing adipogenesis and by keratinocytes, neutrophils, and mast cells in the skin (13, 22, 23). The expression of *Camp* was decreased by stress and restored by ADX (Fig. 4A and fig. S6A), whereas several α -defensin AMPs remained unaltered, and members of the β -defensin family were either unaffected or enhanced. Total *Camp* mRNA in the skin slightly increased by stress during the early phase of SA infection and then decreased at 48 hours (Fig. 4B). Immunohistochemical analysis by costaining of perilesional skin showed that mouse *Camp* protein (CRAMP) was reduced in platelet-derived growth factor receptor A-positive (PDGFRA $^+$) fibroblasts under stress conditions (Fig. 4C), whereas CRAMP in GR1 $^+$ neutrophils remained unchanged (Fig. 4D). Protein immunoblot of total skin extracts showed loss of expression of the 4.8-kDa mature, antimicrobial active CRAMP peptide in response to stress and that this was reversed by ADX (Fig. 4E). These results, combined with observations by immunostaining, suggest that active, mature CRAMP is lost from adipogenic fibroblasts, but neutrophil CRAMP remains intact.

Because neutrophils are a major source of AMPs and are critical for resistance to SA infection, we further studied neutrophil function in the skin during stress. Flow cytometry analyses of skin 3 hours after infection showed that psychological stress during SA infection increased the early recruitment of CD45 $^+$ CD11b $^+$ Ly6G $^+$ neutrophils (Fig. 4, F and G). The early expression of chemokines associated with neutrophil recruitment (*Cxcl1* and *Cxcl2*) and the neutrophil chemokine receptor *Cxcr2* also increased with stress and SA infection (fig. S6B). In blood, stress elicited increased *Camp* expression accompanied by increased bacterial killing activity (Fig. 4, H and I) and increased the expression of chemokine receptors *Cxcr3* and *Cxcr7* (fig. S6C). This, coupled with the observation from scRNA-seq data of enriched phagocytes and positive regulation of defense response pathways in neutrophil clusters (fig. S6D), suggests that the increase in total *Camp* observed in the early phase of infection after stress was likely a reflection of the increased abundance of neutrophils and that the later decrease in *Camp* after stress reflects the suppression of expression in fibroblasts.

To further test whether a change in inflammatory cell recruitment was responsible for increased infection after stress, cyclophosphamide was used to induce neutropenia (fig. S6E). *Cxcr2*, a marker of neutrophils, confirmed that neutrophils were reduced by cyclophosphamide (fig. S6F). However, despite the loss of neutrophils, stress continued to increase SA CFU and the infectious lesion size (Fig. 4) and fig. S6G). Given that AMPs can also recruit and activate T cells to help control inflammation during SA infection (24, 25), we inhibited T lymphocyte egress after stress using fingolimod (FTY720) (fig. S7A). In control mice and those with SA infection, with or without stress, FTY720 suppressed the percentage of T cells in the blood (fig. S7, B and C). Increased neutrophils were observed after FTY720, which were further elevated by stress (fig. S7, D and E). Stress further increased SA infection lesion size in the FTY720-treated mice (fig. S7, F and G) and SA CFU (fig. S7H). The continued increase in infection despite the induction of neutropenia or inhibition of T cell egress suggests that stress exacerbation of SA infection is likely to be attributed to actions on other cell types.

Keratinocytes are also a source of *Camp* in the skin and can be induced in keratinocytes by stimulation with the Toll-like receptor 2 (TLR2)/6 agonist macrophage-activating lipopeptide 2 (MALP2) or

the active form of vitamin D3 (1,25-dihydroxyvitamin D; 1,25VD3). The addition of stress hormones did not cause a discernible change in *Camp* mRNA expression in either primary human keratinocytes or the keratinocyte cell line HaCaT (fig. S8, A and B). In addition, the direct treatment of bacteria in culture with adrenaline, noradrenaline, or corticosterone did not alter the growth of SA (fig. S9A). Stress hormones also did not alter the expression of SA toxins *hla* and *hld* (fig. S9, B and C), nor did stress hormones alter the capacity of SA to induce cytotoxicity when SA-conditioned medium was added to HaCaT keratinocytes (fig. S9D). These results suggest that adrenergic signaling does not result in an alteration in the expression of *Camp* by keratinocytes and that stress hormones do not change the toxic behavior of SA.

Adrenaline inhibits the antimicrobial function of fibroblasts

Because our results showed that stress or adrenaline administration inhibited local adipogenesis and AMP expression in mice, we next directly assessed the influence of stress hormones on preadipocyte fibroblasts in culture. Murine 3T3-L1, the human preadipocyte (HPAd) fibroblast cell lines, and primary mouse dermal fibroblasts were stimulated with adipocyte differentiation medium in culture for 2 days to initiate adipogenesis in the presence or absence of adrenaline. Bulk RNA-seq data from these experiments revealed a distinct transcriptional effect of adrenaline (Fig. 5A). HALLMARK and Kyoto Encyclopedia of Genes and Genomes pathway analysis further indicated that adrenaline suppressed pathways relative to lipid metabolism and adipogenesis in cultured fibroblasts (Fig. 5B and fig. S10A). qPCR analysis showed a reduction in the expression of transcription factors *Pparg* and *Cebpa* associated with preadipocyte differentiation and diminished levels of mature adipocyte markers such as *Adipoq* and *Fabp4* upon exposure to adrenaline (Fig. 5C). The increased expression of cathelicidin in mouse or human fibroblasts triggered by adipogenesis was inhibited in a dose-dependent manner by the addition of adrenaline (Fig. 5D and fig. S10, B and C). Decreases in lipid staining and alterations in cellular morphology, including loss of small lipid droplets, occurred in cultured cells undergoing adipogenesis after exposure to adrenaline (fig. S10, D and E). Both human and mouse preadipocyte cell lines also showed less cathelicidin protein expression by immunostaining (CRAMP in mouse and LL37 in human) (Fig. 5E). To assess whether this was functionally relevant, we tested the supernatant from adrenaline-exposed preadipocytes for its ability to inhibit the growth of an *mprF*-mutant strain of SA (Fig. 5F and fig. S10F). This *mprF* mutant is more susceptible to killing by cathelicidin peptides and provides a more sensitive assay system for antimicrobial activity (26, 27). Inhibition of α -adrenergic signaling restored the expression of *Camp* and decreased the growth of *mprF*-mutant SA in the supernatant from adrenaline-exposed adipocytes (fig. S10, G and H).

Having established in vitro that adrenaline can inhibit the capacity of preadipocyte fibroblasts to express *Camp* and inhibit SA, we next assessed the relative contribution of *Camp* from fibroblasts in vivo during SA infection. *Camp* was deleted in all fibroblasts by crossing *Camp* ff mice with *Pdgfra*-cre mice (*Pdgfra* $^{\Delta Camp}$). *Pdgfra* $^{\Delta Camp}$ mice lacked *Camp* expression in fibroblasts, but no loss of expression of *Camp* could be detected in cells extracted from the bone marrow (fig. S11A). Immunostaining of mouse skin for CRAMP and PDGFRA showed colocalization of CRAMP in fibroblasts after infection in control mice but loss of fibroblast-associated CRAMP in *Pdgfra* $^{\Delta Camp}$ mice (fig. S11B). These *Pdgfra* $^{\Delta Camp}$ mice were

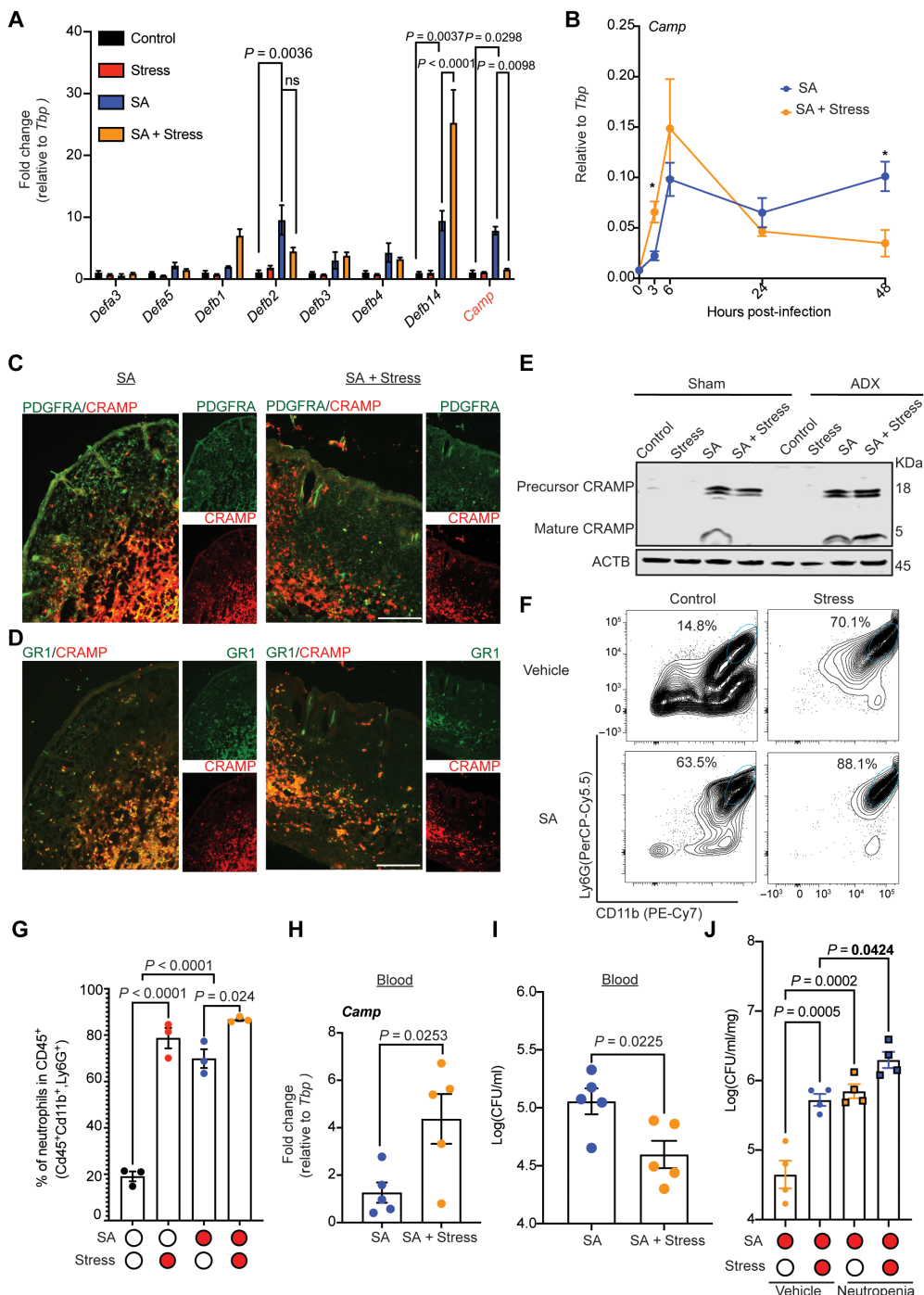


Fig. 4. Psychological stress exacerbates SA infection via suppression of cathelicidin. (A) Gene expression based on qPCR analysis for AMPs (α -defensin, β -defensin, and *Camp*) of whole skin at day 2 with and without SA infection and with or without stress or ADX (three to six per each condition). (B) Time course of *Camp* expression after SA infection with or without stress (three to six per each condition). * $P < 0.05$. (C) Immunohistochemical images of perilesional skin showing CRAMP protein expression (red) and fibroblasts (PDGFR α ; green) 2 days after SA infection or SA with stress (representative of $n = 3$ per each condition). Scale bar, 300 μ m. (D) Immunohistochemical images of perilesional skin showing CRAMP protein expression (red) and neutrophils (GR1; green) 2 days after SA infection or SA with stress (representative of $n = 3$ per each condition; large box is costained images, and small boxes show individual stains). Scale bar, 300 μ m. (E) Protein immunoblot of mouse cathelicidin (CRAMP) and actin from skin 2 days after SA infection, SA infection with stress, or these conditions after ADX. (F) Flow cytometry plots for Ly6G and CD11b in the skin at 3 hours postinfection of SA-infected mice with and without stress ($n = 3$ per group). (G) Qualification of the percentage of neutrophils from (F) (gated as viable CD45 $^+$ Ly6G $^+$ CD11b $^+$ cells). (H) Whole-blood mouse mRNA expression of AMP *Camp* in SA infection with or without psychological stress at day 2 ($n = 5$ per each condition). (I) Whole-blood killing activity against SA in blood from mice with or without psychological stress at day 2 after infection ($n = 5$ per each condition). (J) Effect of chemical neutropenia on the response to stress as measured by SA CFU/ml per mg of tissue ($n = 4$ mice for each condition). Results in all panels are represented as means \pm SEM from two or more independent experiments. Significance was calculated using a one-way ANOVA (three or more group comparisons) or unpaired Student's *t* test (two groups).

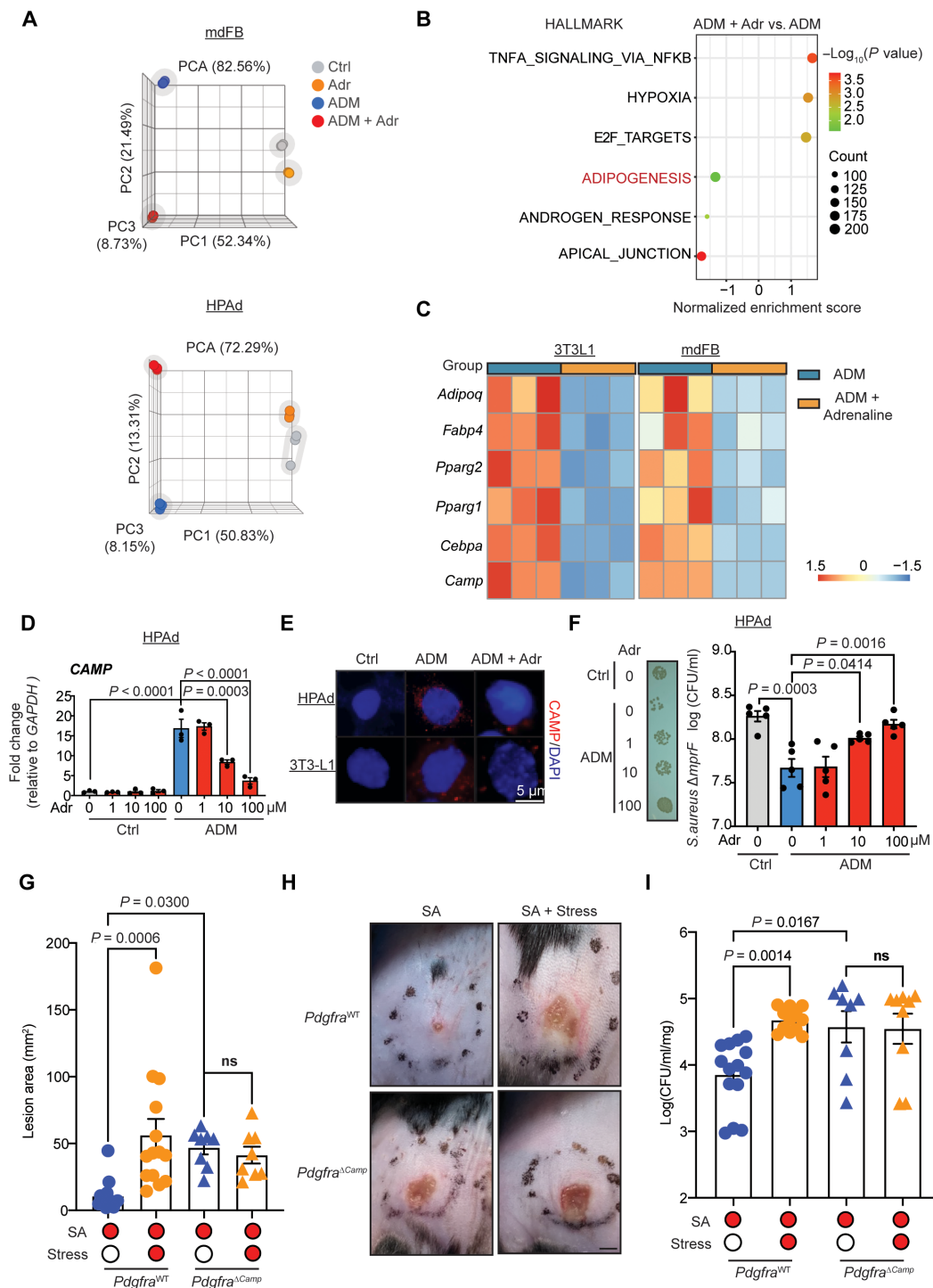


Fig. 5. Adrenaline inhibits cathelicidin expression by preadipocytes. (A) PCA of normalized bulk RNA-seq data for mdFBs or HPAd treated with Adr or adipocyte differentiation medium (ADM) in the absence or presence of Adr ($n = 3$ per group). (B) Enrichment analysis of HALLMARK database (false discovery rate < 0.05) of related pathways under the indicated conditions. (C) Heatmap display of qPCR results for the expression of genes involved in adipogenesis by mouse fibroblasts (3T3L1 and mdFB) in response to adipocyte differentiation medium in the presence or absence of Adr for 2 days in comparison with control (representative of $n = 3$ per group). (D) Camp expression in HPAd with adipocyte differentiation medium in the presence or absence of various concentrations of Adr ($n = 3$ per each condition). (E) Representative CAMP staining (red) and DAPI (blue) in HPAd and 3T3L1 cells grown in adipocyte differentiation medium in the presence or absence of Adr. Scale bar, 5 μ M (representative of $n = 3$ per group). (F) Bacterial growth on agar plate and CFUs of $S. aureus$ Δ mpf after 48-hour exposure to conditioned medium from preadipocytes treated with Adr as indicated ($n = 5$ per each condition). (G) Comparison of 2-day SA lesion size from *Pdgfra*^{WT} mice or *Pdgfra*^{ΔCamp} mice in the absence or presence of stress ($n = 8$ to 14 lesions from four to seven mice for each condition). (H) Representative photograph of lesions from (G). Scale bar, 1.5 mm. (I) SA CFU in skin tissue from experiments shown in (G) (8 to 14 lesions from four to seven mice for each condition). Results in all panels are represented as means \pm SEM from two or more independent experiments. Significance was calculated using a one-way ANOVA (three or more group comparisons); ns, not significant.

significantly more susceptible to SA infection compared with wild-type (WT) littermate controls but had no further increase in SA infection after stress (Fig. 5, G to I). These results support the conclusion that the increase in SA infection by stress acts through *Camp*-producing fibroblasts.

Psychological stress acts through TGF β to inhibit local host defense

To determine the mechanism through which stress can inhibit the ability of fibroblasts to protect against SA infection, we next returned to our scRNA-seq data for an analysis of intercellular receptor-ligand pairs via CellChat (Fig. 6A and fig. S12A) (28). Among all cells, this analysis showed that several signaling pathways, including insulin-like growth factor (IGF) and KIT, were inhibited in mice during psychological stress (Fig. 6A). The IGF signaling pathway constitutes a well-established molecular cascade that facilitates adipogenesis by orchestrating a lineage bias in endogenous adipose stem/progenitor cells (29, 30), and KIT signaling is known to enhance the expression of lipogenic enzymes, facilitating lipid accumulation in adipocytes (31). On the other hand, the top three enriched signaling pathways in the stress-exposed group were interleukin-1 (IL-1), colony-stimulating factor (CSF), and TGF β (Fig. 6A). An increase in local IL-1 or CSF signaling is not likely to explain the increased susceptibility to infection given that both pathways have been shown to improve defense against SA (32, 33). However, because TGF β has been associated with inhibition of reactive adipogenesis (12, 13, 34, 35) and may not be detected in this analysis of all cells, the TGF β pathway was explored further in an attempt to explain the increased susceptibility to infection after stress.

Higher circulating concentrations of TGF β 1 and TGF β 2 were seen in mice after stress (Fig. 6B), and the increased expression of *Tgfb1* and *Tgfb3* was seen in the skin (Fig. 6C). Further analysis of the sources of *Tgfb1* and *Tgfb3* by scRNA-seq revealed that *Tgfb1* is primarily expressed by neutrophils, macrophages, T helper 17 cells, and $\gamma\delta$ T cells, whereas *Tgfb3* is predominantly expressed by macrophages (fig. S12B). Increased activity of the TGF β pathway is further supported by top three GSEA from bulk RNA-seq, showing inhibition of type I interferons (IFN- α/β) (36), which is restored by ADX (fig. S12C). Stressed mice also had an increase in genes associated with fibrosis and inflammation (*Ccn2*, *Spp1*, and *Il6*) (Fig. 6C). Immunofluorescence staining confirmed the increased presence of TGF β as seen by pan-TGF β -positive staining in fibroblasts located in the upper papillary dermises of stressed mice compared with those of nonstressed mice (Fig. 6D). The analysis of scRNA-seq results from the skin also showed an increase in several TGF β family members (*Tgfb2* and *Tgfb3*) and receptor genes (*Acvr1* and *Tgfb2r2*) in fibroblasts upon stress (Fig. 6E). The transcriptional profile of stress-elicited fibroblasts indicated a high degree of SMAD binding (*Hmga2*, *Zmiz1*, and *Acvr1b*) inferred from GO analysis (Fig. 6F). Up-regulation of pathways “TGF β receptor signaling in epithelial-mesenchymal-transition (EMT) epithelial to mesenchymal transition” and “TGF β family members” was also observed after stress in Reactome pathway enrichment by using AUCell score (fig. S12D). The examination of the individual contributions of each ligand-receptor pair to the TGF β signaling pathway suggested that TGF β originated from diverse sources such as adipocytes, lymphoid cells, and endothelial cells, with fibroblasts emerging as the predominant target receptor in the context of stress (fig. S12E).

Further examination of fibroblast subpopulations (fig. S13, A to D) revealed that, as depicted in fig. S13B, the F3 and F4 subsets contained

several highly expressed TGF β downstream genes, including *phosphodiesterase 2* (*Enpp2*) and *semaphorin 3A* (*Sema3a*) (37, 38), whereas the F0 and F5 subset contained several highly expressed adipogenesis-associated genes, including *matrix gla protein* (*Mgp*), *C-C motif chemokine ligand 2* (*Ccl2*), and *prostaglandin-endoperoxide synthase* (*Ptg2*) (39–41). F0, F2, and F5 fibroblasts that exhibit traits of both preadipocyte fibroblasts (42–44) and inflammatory fibroblasts (45) are highly depleted after stress. Meanwhile, clusters F3 and F4 were markedly enriched by stress, displaying myofibroblast features (fig. S13, C and D) (46). Furthermore, GO enrichment analysis indicated a loss of proadipogenic potential and antimicrobial humoral immune response mediated by AMP and activation of the TGF β /SMAD pathway associated with fibroblast subsets that are enriched in stress-exposed SA-infected skin (fig. S13E). In the fibroblast cell culture model, we also observed that treatment of human or mouse fibroblasts with adrenaline resulted in increased expression of TGF β 1, TGF β 2, and TGF β 3 and a concomitant elevation in TGF β 1 protein levels within preadipocytes (Fig. 6, G and H, and fig. S13F) and the TGF β target genes (fig. S13G) (47–49). Combined, these data strongly suggest that stress activates TGF β signaling in fibroblasts.

To test whether TGF β is required for stress to suppress local innate defenses against SA, we next interfered with TGF β signaling in mice during stress by using either a potent pan-TGF β -neutralizing antibody (neutralizes all TGF β isoforms) or a TGF β receptor (TGF β R) antagonist (SB431542) (Fig. 7A). Either intervention reversed the increased susceptibility to SA infection and decreased the survival of SA in the skin of stressed mice (Fig. 7, B to G). SB431542-treated mice did not show significant changes in plasma adrenaline (fig. S14A). Moreover, both the pan-TGF β -neutralizing antibody and the TGF β R inhibitor exhibited comparable effects in restoring dermal adipose expansion in stressed mice as evidenced by increased subcutaneous adipose layer and lipid accumulation (Fig. 7, H to K, and fig. S14, B and C). In addition, the expression of pro-adipogenic genes (*Pparg*, *Cebp*, *Adipoq*, and *Camp*) increased with the administration of either the TGF β R inhibitor or pan-TGF β -neutralizing antibody (fig. S14, D to F). Profibrotic genes (*Spp1* and *Il6*) were also restored by pan-TGF β -neutralizing antibody (fig. S14G). Inhibition of TGF β R did not block stress-related weight loss (fig. S14, H and I). Moreover, the direct administration of recombinant TGF β 1 (rTGF β 1) was sufficient to increase susceptibility to SA infection and increase survival of SA in the skin (fig. S15, A to C).

To confirm that fibroblasts were responsible for the effects of TGF β on infection, we generated a conditional tamoxifen-inducible Cre-driven deletion of *Tgfb2* by crossing *Tgfb2*^{fl/fl} mice with *Pdgfra-creERT2* mice (*Pdgfra*^{ΔTgfb2}) (fig. S15D). Dermal fibroblasts isolated from mice after administration of tamoxifen (*Pdgfra*^{ΔTgfb2}) demonstrated efficient knockdown of *Tgfb2* without detectable knockdown in the epidermis, blood, or spleen (fig. S15E). *Pdgfra*^{ΔTgfb2} mice gained resistance to SA infection under stress, as evidenced by reduced lesion sizes (Fig. 7, L and M), diminished SA survival in the skin (Fig. 7N), and increased expression of proadipogenic genes (*Pparg2* and *Camp*) (fig. S15, F and G). These observations confirm that the action of TGF β on fibroblasts was responsible for the increased susceptibility to SA infection caused by stress.

DISCUSSION

Psychological stress triggers a beneficial fight-or-flight response that can enhance survival under some contexts but is also strongly associated with increased severity of infections, some of which can be

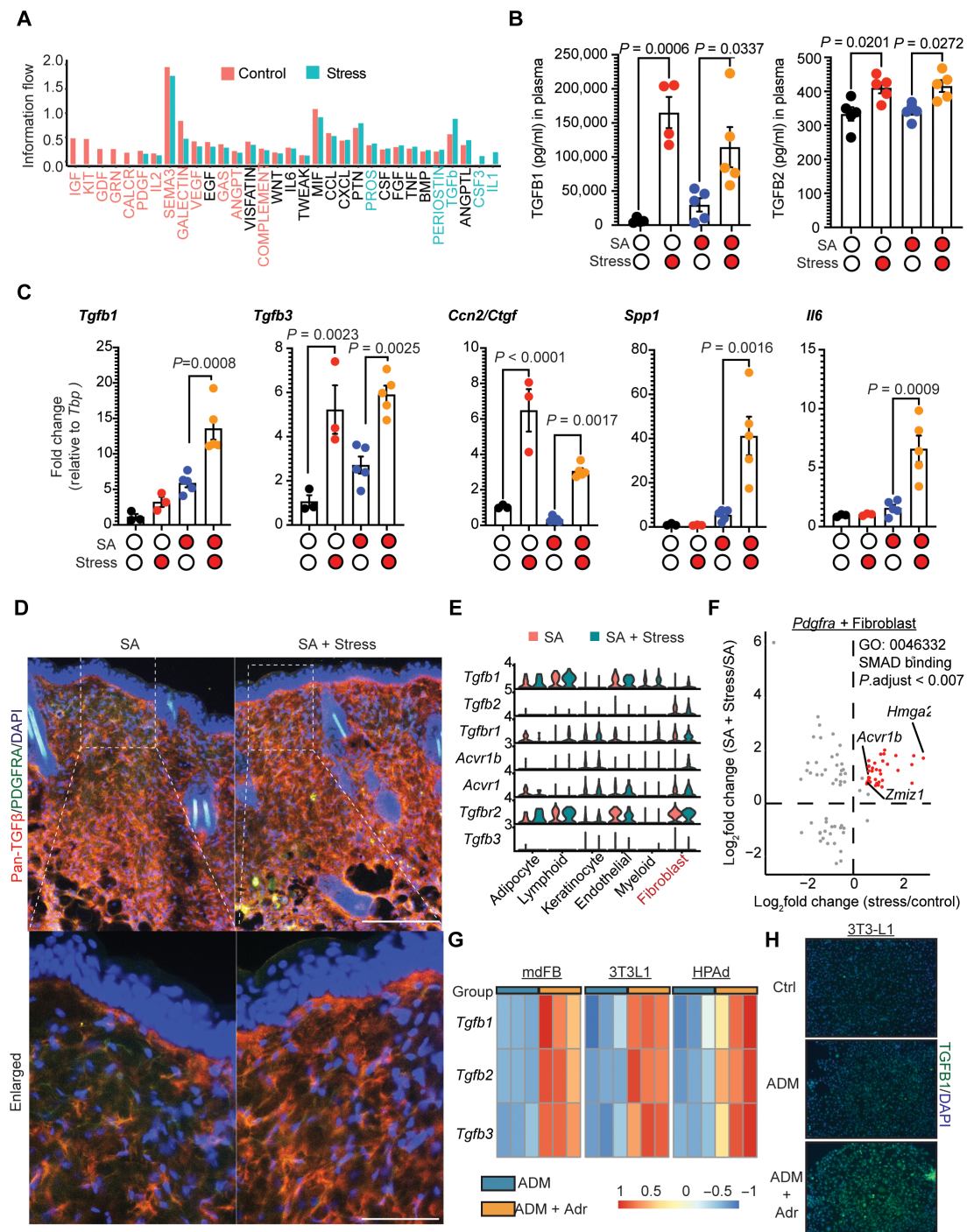


Fig. 6. Psychological stress induces TGF β expression and activates the TGF β pathway in dermal fibroblasts. (A) Analysis of scRNA-seq data for signaling pathways underlying interactions of all cells isolated from mouse skin after stress compared with control. (B) Measurement of plasma concentrations of TGF β 1 or TGF β 2 in mice for the indicated group ($n = 4$ or 5 per each condition). (C) qPCR analysis of mRNA in skin for *Tgfb1*, *Tgfb3*, *Ccn2/Ctgf*, *Spp1*, and *Il6* in the indicated groups ($n = 3$ to 5 mice for each condition). (D) Immunohistochemical staining of skin with pan-TGF β (red) and PDGFR α (green) antibodies under the indicated condition (representative of $n = 3$ per each condition). Nuclei were counterstained with DAPI (blue). The lower row is an enlarged image from the area indicated by a dotted white line. Scale bars, 300 μ m and 50 μ m (enlarged). (E) Violin plots showing the expression of the *Tgfb1*, *Tgfb2*, *Tgfb3*, *Tgfb1b*, *Acvr1b*, *Acvr1*, and *Tgfb2r* genes in all clusters in the context of SA infection with or without stress. (F) Average log₂ fold change expression of significantly regulated genes in SA-infected plus stress compared with control in *Pdgfra* + fibroblasts. (G) Heatmap showing relative mRNA expression (based on RT-qPCR and relative to control condition) of TGF β isoforms in mdFB, 3T3L1, and HPAad preadipocytes with ADM in the presence or absence of Adr ($n = 3$ for each condition). (H) Representative TGF β 1 staining in 3T3L1 treated with adipocyte differentiation medium in the presence or absence of Adr. Nuclei were counterstained with DAPI (blue). Scale bar, 750 μ m. Results in all panels are shown as means \pm SEM from two or more independent experiments. Significance was calculated using a one-way ANOVA (three or more group comparisons).

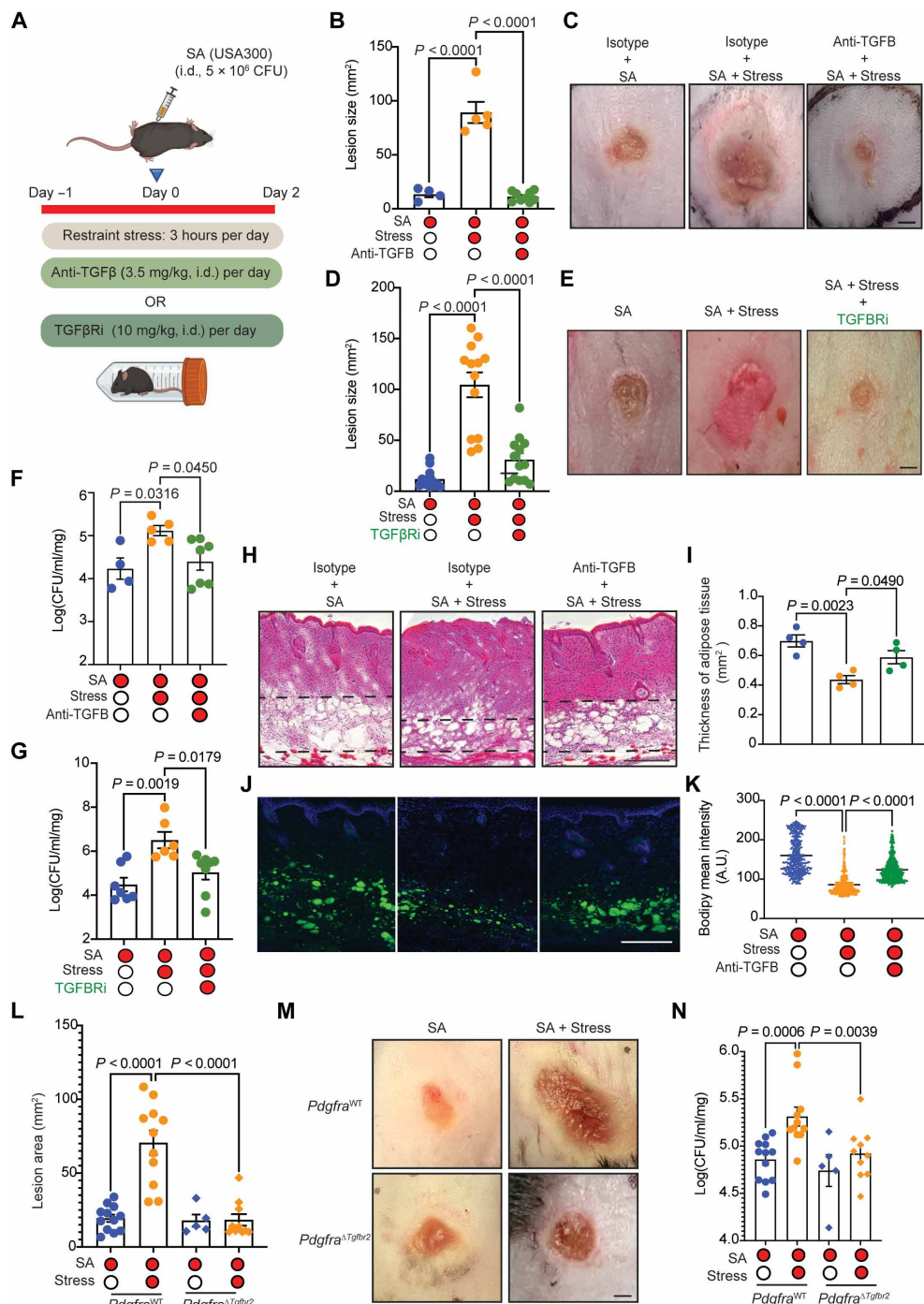


Fig. 7. Inhibition of TGF β pathway restores resistance to SA infection during psychological stress. (A) Schematic illustration of experimental design assessing pan-TGF β -neutralizing antibody and TGF β receptor inhibitor (TGF β Ri) during stress and SA infection. (B) SA lesion size measured at day 2 after SA injection with or without stress or pan-TGF β -neutralizing antibody with stress ($n = 4$ to 9 lesions from three to five mice for each condition). (C) Representative photograph of lesions from (B). Scale bar, 1.5 mm. (D) SA lesion size measured at day 2 after SA injection with or without stress or pretreatment with TGF β receptor inhibitor plus stress ($n = 12$ or 13 lesions from six or seven mice for each condition). (E) Representative photograph of lesions from (D). Scale bar, 1.5 mm. (F) SA CFU in skin tissue from experiments shown in (B) ($n = 4$ to 7 lesions from four mice for each condition). (G) SA CFU in skin tissue from experiments shown in (D) ($n = 6$ to 8 lesions from three or four mice for each condition). (H) Skin biopsies at day 2 after SA infection were collected for H&E staining as indicated. Adipose layer is marked with dashed lines (representative of $n = 3$ per group). Scale bar, 300 μ m. (I) Quantification of adipose tissue thickness shown in (H) ($n = 4$ per group). Nuclei were stained by DAPI (blue). Scale bar, 300 μ m. (K) Quantification of the mean intensity of lipid droplets in (J) ($n = 466$ for SA; $n = 398$ for SA with stress; $n = 698$ for SA with stress plus pan-TGF β -neutralizing antibody). (L) Comparison of 2-day SA lesion size from Pdgfra WT mice or Pdgfra $^{\Delta Tgfb2}$ mice in the absence or presence of stress ($n = 5$ to 12 lesions from three to six mice for each condition). (M) Representative photograph of lesions from (L). Scale bar, 1.5 mm. (N) SA CFU in skin tissue from experiments shown in (L) (5 to 12 lesions from three to six mice for each condition). Results in all panels are represented as means \pm SEM from two or more independent experiments. Significance was calculated using a one-way ANOVA (three or more group comparisons).

life threatening (50, 51). Considerable prior work has identified that stress can diminish functions of various aspects of the immune system but has been biased by focusing on some specific cell types (e.g., immune cells) and testing preconceived hypotheses. Now, it is recognized that several other cell types participate in the antimicrobial defense against SA, including keratinocytes, mast cells, and fibroblasts (52–55). Here, by initiating an unbiased analysis of the skin during SA infection, we identify that dermal fibroblasts are an important cell type responding to SA and appear to be the primary cell responsible for the large increase in deep skin infection by SA that occurs after severe psychological stress. This approach provides a road map to explore alternative approaches to support immune protection and identifies that fibroblasts and TGF β mediate this important event.

Acute stress induces changes in the trafficking, maturation, and function of dendritic cells, neutrophils, macrophages, and lymphocytes through the activation of adrenoceptors on these cells (56, 57). Catecholamines inhibit cytokine production and proliferation from T cells (9), whereas adrenaline boosts immune responses in macrophages (58). Hypercortisolemia and irregular cortisol patterns are known to weaken the immune system and increase the susceptibility to opportunistic infections such as bacteremia and sepsis (59, 60). However, we show here that mice after ADX have lower levels of corticosterone compared with sham-operated mice yet exhibit responses to SA infection similar to those of sham-operated control mice after stress. This suggests that corticosterone has a lesser effect on deep tissue infection in this model or may differ between local skin infections and systemic infections.

The current observations strongly suggest that dermal fibroblasts play a major role in the increase in SA infection of the skin during stress. Such an important role for fibroblasts in SA infection was unexpected because neutrophil recruitment is the most well-recognized cell type to limit infection by SA (61). Furthermore, $\gamma\delta$ T cells contribute to host defense, and acute stress leads to lymphocyte redistribution (62, 63). However, in our study, stress enhanced the expansion of $\gamma\delta$ T cells in the skin, increased the early recruitment of neutrophils to the site of SA infection, and enhanced the capacity of neutrophils to inhibit SA growth in a blood-killing assay. Chemically induced cytopenia by cycloheximide or decreasing mobilization of T cells with fingolimod did not mitigate the capacity of stress to increase SA infection. Therefore, these observations suggest that the action of stress to inhibit host defense against SA is not mediated by neutrophils and lymphocytes and that another cell type is active in this system.

We found that stress decreases the expression of *Camp*, which is an essential effector molecule to fight against bacterial infections (64–66). Several cell types express *Camp*, including neutrophils, keratinocytes, and dermal fibroblasts undergoing adipogenesis (12, 67, 68). Stress can reduce *Camp* in keratinocytes by activating nicotinic receptors and can lead to increased infection by group A *Streptococcus* (69). In this model of SA infection, we found that stress also suppresses the expression of *Camp* in fibroblasts. Although *Camp* protein expression was unchanged in neutrophils, the targeted deletion of *Camp* in fibroblasts demonstrated that producing the AMP from these cells is important. The mechanism for suppression of AMP expression is complex and may also involve nicotinic receptors given that they stimulate a positive feedback loop for catecholamine stimulation and activation of adrenergic signaling (70, 71). Thus, in addition to the direct effects of adrenaline on fibroblasts, other signals may also affect the antimicrobial activity mediated by fibroblasts.

This investigation also unexpectedly reveals that psychological stress triggers activation of TGF β signaling, leading to decreased *Camp* expression by fibroblasts. Although, to our knowledge, TGF β has not been previously reported to drive infections during stress, our findings are consistent with its reported influence on the proliferation, survival, activation, and differentiation of immune cells (72) and its adverse effects on bacterial and viral infections (73, 74). We showed that a TGF β pan-neutralizing antibody or a TGF β R inhibitor restores normal antimicrobial functions and enhances resistance to SA in stressed mice. Functionally, the TGF β R inhibitor suppressed TGF β 1 expression in neutrophils, macrophages, and $\gamma\delta$ T cells (fig. S11B). Given the pleiotropic effects of TGF β , we then used fibroblast-specific deletion of *Tgfb2*. Improved resistance to infection in these mice further demonstrates the role of fibroblasts and TGF β during SA infection and stress.

Members of the TGF β family are expressed by several cells in the skin, including lymphocytes, macrophages, and fibroblasts (75). Furthermore, stress can induce lymphocyte apoptosis by altering CD95 expression (76) and subsequently stimulating TGF β 1 (77). In addition, enteric neurons exposed to stress stimulate the release of TGF β 2 in models of intestinal inflammation (15). Noradrenaline has been reported to have a synergistic effect on TGF β signaling in cardiac fibrosis (78), and stress can inhibit adipogenesis by up-regulating cytokines such as IL-6 and tumor necrosis factor, thereby promoting lipolysis of adipocytes and fat loss (79–82). Thus, the events linking stress, the HPA axis, activation of TGF β signaling, and our observations of dysfunction of fibroblast immune function during adipogenesis are complex and require further study.

These observations have potentially important clinical implications for treating infections, particularly in the setting of stress. Xanax (alprazolam) exerts its calming effects through central nervous system modulation but is not currently indicated for treating infections. By suppressing HPA axis activity, Xanax may reduce adrenaline levels and subsequently TGF β signaling, a pathway that could theoretically affect the host response to bacterial infections (83). The use of inhibitors of adrenergic signaling, such as propranolol, or the specific use of inhibitors of TGF β also warrants consideration.

This study presents some limitations that should be noted. First, our findings were derived from cell lines and murine model experiments. Further investigation involving human participants is imperative for comprehensive understanding. Second, scRNA-seq analysis fails to assess the transcriptional profile of cells not easily recovered during the isolation process, such as granulocytes and adipocytes, and may therefore overrepresent the relative contribution of fibroblasts. scRNA-seq also has limited capacity to detect some transcripts, including *Camp*, and thus additional analysis methods must be used to measure the expression of this gene. Third, the structural similarity between noradrenaline and adrenaline suggests a potential role of noradrenaline in inhibiting fibroblast-mediated CAMP activity. Last, the *Pdgfra-cre* mouse line also is active in retinal cells, oligodendrocytes, and some other mesenchymal cell types (84, 85); thus, the interpretation of results should consider the potential contribution of these cells when interpreting results of *Pdgfra-Cre*-targeted deletion in fibroblasts. In addition, differences in *Pparg* expression could also arise from sebaceous glands (86). Notwithstanding these limitations, our data strongly support the critical role of dermal fibroblasts and TGF β in stress-related skin bacterial infections.

MATERIALS AND METHODS

Study design

This study investigated how psychological stress affects susceptibility to bacterial infections. Restraint stress was used to model psychological stress, and SA infection was used to assess changes in infection susceptibility. We used bulk RNA-seq, scRNA-seq, and lipidomics to analyze the molecular responses. Fibroblast-specific *Camp* knockout mice and pharmacological inhibitors of TGF β signaling were used to examine how stress-induced alterations in fibroblast function contribute to infection susceptibility. Our findings revealed that stress activates TGF β signaling in fibroblasts, leading to the suppression of *Camp* expression and an increase in infection susceptibility. The sizes of the experimental groups and the number of cohorts are detailed in the figure legends.

Mouse model of SA skin infection

Skin infection experiments were undertaken in accordance with established protocols (11). SA strain USA300/methicillin-resistant SA was used for in vivo infection experiments. In brief, the backs of adult WT mice of matched sex and age or specific mutant strains were shaved, and hair was removed using chemical depilation (Nair). After this, they were subcutaneously injected with 100 μ l of mid-logarithmic growth phase SA (5×10^6 CFU of bacteria) in phosphate-buffered saline (PBS). On day 2, mice were euthanized, and an 8-mm skin punch biopsy was taken from the center of the infection. In addition, skin surrounding the abscess center (6 to 8 mm) that lacked abscess formation was meticulously dissected for RNA extraction or CFU determination. Skin biopsies were homogenized in 1 ml of PureLink RNA lysis buffer (Thermo Fisher Scientific, 12183025) or PBS (for CFU counting) using 2-mm zirconia beads (BioSpec, 11079124zx) in a mini-bead beater 16 (Thermo Fisher Scientific, NC0261884). For CFU quantification, half of the homogenized skin samples were serially diluted, plated onto tryptic soy agar (TSB) (Thermo Fisher Scientific, MT61411RO), and enumerated after 18 hours to determine the CFU/ml per gram of tissue.

Restraint stress model

To induce restraint stress, mice were confined within 50-ml polypropylene conical tubes fitted with ventilation caps for 3 hours a day on 3 consecutive days. These stress sessions commenced each day between 12 p.m. and 3 p.m. On the day of SA infection (day 0), restraint stress was performed immediately after intradermal injection of SA.

Adrenalectomy

ADX was performed according to established procedures (87). C57BL/6J mice, aged 6 weeks, were anesthetized, and small incisions were made on the dorsal skin directly above each adrenal gland. Using curved forceps, both adrenal glands were excised. Sham-operated mice (sham) underwent the same procedures as the ADX mice, except that their adrenal glands were not removed. To compensate for the loss of aldosterone production due to adrenal gland removal, both ADX and sham mice had their drinking water supplemented with a 1% (w/v) saline solution, because aldosterone plays a role in maintaining salt balance.

Neutropenic model

Neutropenia was induced as described previously (88). Cyclophosphamide (Cayman, 13849) was dissolved in distilled water for injection. Mice received a cumulative dose of 250 mg/kg through two

intraperitoneal injections, each at a volume of 0.5 ml. The injections were administered on day -5 with a dose of 150 mg/kg, followed by a dose of 100 mg/kg on day -2 before the commencement of restraint stress.

Sympathetic nerve ablation model

To ablate sympathetic nerves, a solution of 6-OHDA hydrobromide (Sigma-Aldrich, H4381) was freshly prepared by dissolving 6-OHDA in 0.1% ascorbic acid in 0.9% sterile NaCl. Mice received intraperitoneal injections of 6-OHDA at a dose of 150 mg/kg of body weight, followed by another injection of 100 mg/kg of body weight on 2 consecutive days. Mice were allowed to recover for 5 days before the initiation of restraint stress. Control mice were injected with an equivalent volume of vehicle (0.1% ascorbic acid in 0.9% sterile NaCl).

Animals and animal care

All animal experiments conducted were approved by the University of California, San Diego (UCSD), Institutional Animal Care and Use Committee. C57BL/6 WT mice (RRID: MGI:2159769) were initially obtained from the Jackson Laboratory and subsequently bred and housed in the animal facility at UCSD. *Pdgfra*-cre (RRID:IMSR_JAX:013148), *Pdgfra*-CreERT2 (RRID:IMSR_JAX:032770), and *Tgfb2*^{fl/fl} (RRID:IMSR_JAX:012603) mice were originally purchased from the Jackson Laboratory and bred and maintained in the UCSD animal facility. *Camp*^{fl/fl} mice, where exon 2 and exon 4 of the *Camp* gene were flanked by LoxP sites, were generated as previously described (12). Fibroblast-specific deletion of *Camp* and *Tgfb2* were achieved by crossing *Camp*^{fl/fl} mice with *Pdgfra*-cre mice and *Tgfb2*^{fl/fl} mice with *Pdgfra*-CreERT2 mice, respectively.

Cell lines

The primary mouse preadipocyte cell line 3 T3-L1 (American Type Culture Collection, CL-173), primary human preadipocytes HPAd cells (Cell Applications, 802 s-05a), and immortalized human keratinocytes (HaCaT) cells were cultured in Dulbecco's modified Eagle's medium with glucose (4.5 g/liter; Thermo Fisher Scientific, 11995073) supplemented with 10% fetal bovine serum (Thermo Fisher Scientific, SH3091003HI), 2 mM L-glutamine (Thermo Fisher Scientific, 35050061), and penicillin (50 U/ml) and streptomycin (50 μ g/ml; Thermo Fisher Scientific, 15140122). Normal human keratinocytes (Thermo Fisher Scientific, C0015C) were cultured in EpiLife medium (Thermo Fisher Scientific, MEPI500CA) supplemented with 0.06 mM calcium, EpiLife defined growth supplement (EDGS) (Thermo Fisher Scientific, S0125), and penicillin/streptomycin. All of these cell lines were maintained in a humidified atmosphere containing 5% CO₂.

Bacterial strains

SA (USA300) and SA Δ *mprF* were cultured in tryptic soy broth (Thermo Fisher Scientific, MT61411RO) at 37°C under aerobic conditions for 24 hours before use.

Flow cytometry and analysis

Mouse dorsal skin was initially stained with Zombie Violet viability dye (BioLegend, 423114) to label dead cells. Subsequently, cells were blocked using anti-mouse CD16/32 (eBioscience, 14016185) and then stained with an antibody mixture comprising Ly6G-peridinin-chlorophyll-protein-Cy5.5 (BioLegend, 127616) and CD11b-PE-Cy7 (BioLegend, 101216) or CD3e-phycerythrin (PE)-A (Thermo

Fisher Scientific, 12-0031-82) and CD45–PE–Texas Red (Invitrogen, MCD4517). After staining, cells were fixed using stabilizing Fixative buffer (BD Biosciences, 664907). Protein expression analysis of each cell marker was performed using the BD FACSCanto RUO machine, and data were analyzed using FlowJo V10 software. Dead cells, identified by positive staining with Zombie Violet dye, were excluded from the analyses. The gating strategies are summarized in fig. S16.

Reverse transcription–qPCR (RT-qPCR) analyses

Total cellular RNA was extracted using the PureLink RNA Isolation Kit with ribonuclease-free deoxyribonuclease I (Sigma-Aldrich, 4716728001) digestion to eliminate genomic DNA contamination (QIAGEN). Subsequently, 500 ng of RNA was reverse-transcribed to cDNA using the Verso cDNA synthesis kit (Thermo Fisher Scientific, AB1453B). Quantitative real-time PCR was conducted on the CFX96 real-time system (Bio-Rad) using SYBR green mix (Biomiga, QP1311-02). All primers used with SYBR green were designed to span at least one exon to minimize the possibility of nonspecific amplification from genomic DNA. The expression of the *Tbp* gene (*TATA-box binding protein*) was used as a housekeeping gene to normalize data for the expression of mouse genes, whereas *GAPDH* was used as a housekeeping gene for the expression of human genes. Specific primer sequences are provided in table S1.

Protein extraction

Mouse tissue biopsies or cultured 3T3-L1 cells, as well as mouse dermal fibroblasts (mdFBs), were lysed in radioimmunoprecipitation assay buffer (Cell Signaling Technology, #9806) supplemented with a complete proteinase and phosphatase inhibitor cocktail (Thermo Fisher Scientific, A32959) as previously described (89). Protein concentrations were determined using a bicinchoninic acid protein assay kit (Thermo Fisher Scientific, A55864).

Histology, IHC, and immunocytochemistry staining

Tissue biopsies were directly embedded in optimal cutting temperature embedding medium (Thermo Fisher Scientific, 23730571), and frozen sections were fixed in 4% paraformaldehyde (Thermo Fisher Scientific, AA433689M) for 10 min before undergoing hematoxylin and eosin staining (Mercedes Scientific, MER 47991L for hematoxylin; Sigma-Aldrich, HT110116-500 for eosin Y) or immunofluorescence staining. For immunohistochemistry (IHC), fixed and permeabilized tissue sections were blocked with Image-it FX reagent (Thermo Fisher Scientific, R37107) before being incubated with primary antibodies, followed by appropriate 488- or Cy3-coupled secondary antibodies as mentioned in the key resources table. Nuclei were counter-stained with 4',6-diamidino-2-phenylindole (DAPI) (Thermo Fisher Scientific, P36935). All images were captured using an Olympus BX41 microscope.

Primary preadipocytes culture

To induce differentiation, 2 days postconfluent 3T3-L1 or HPAd cells were switched to adipocyte differentiation medium containing 2 mM dexamethasone (Abcam, ab120743), 250 μM 3-isobutyl-1-methylxanthine (Sigma-Aldrich, I5879), 200 μM indomethacin (Sigma-Aldrich, I7378), and recombinant human insulin (10 μg/ml; Sigma-Aldrich, 91077C). Fresh differentiation medium was replenished every other day during the differentiation process, and fresh medium was changed every other day before RNA or protein extraction. Cells from passages 4 to 7 were used for in vitro differentiation.

Keratinocyte stimulation

Cells were stimulated for 24 hours either separately or in combination with the following reagents: 1 nM 1,25 (OH)₂ vitamin D₃ (Sigma-Aldrich, D1530), MALP-2 (100 ng/ml; Enzo Life Sciences, ALX-162-027-C050), 10 nM acetylcholine (Sigma-Aldrich, A6625), 10 μM corticosterone (Sigma-Aldrich, C2505), and 10 μM epinephrine (Cayman Chemical, 18626).

In vitro bacterial killing assay

Conditioned medium devoid of antibiotics and phenol red was obtained from differentiating dermal fibroblasts, following the methodology outlined in a previous study. Subsequently, 100 μl of this conditioned medium was combined with 10⁵ CFU/ml of the specified bacterial strain in 96-well tissue culture microtiter plates. The plates were then incubated at 37°C for durations ranging from 10 to 48 hours before being plated for CFU enumeration. In addition, the optical density at 595 nm was measured daily using a spectrometer.

TGFβ1 and TGFβ2 ELISA

Mouse TGFβ1 concentrations in cell lysates from primary mouse dermal fibroblasts, 3T3L1 cells, or mouse plasma were quantified using the mouse TGFβ1 enzyme-linked immunosorbent assay (ELISA) kit (R&D Systems, DY1679-05), whereas TGFβ2 concentrations were assessed using the TGFβ2 ELISA kit (Thermo Fisher Scientific, MB200). These measurements were performed according to the respective manufacturer's instructions.

Epinephrine/Norepinephrine ELISA Kit

Epinephrine and norepinephrine concentrations in plasma samples were assessed using an epinephrine/norepinephrine ELISA kit (Abnova, KA1877), whereas norepinephrine concentrations in spleen tissue lysates were measured using a noradrenaline high sensitive (Research) ELISA (IBL-America, IB89537R), following the respective manufacturer's instructions.

Corticosterone ELISA Kit

Corticosterone concentrations in plasma samples were determined using the corticosterone ELISA kit (Enzo Life Sciences, ADI-900-097) following the manufacturer's instructions.

Whole blood killing assay

Fresh mouse blood was collected into blood collection tubes containing EDTA (1.5 mg/ml of blood; Thermo Fisher Scientific, 15575020). Next, 10² CFU of freshly diluted log-phase SA (suspended in 10 μl of RPMI medium) was added to 35 μl of blood per well within a 96-well format. This mixture was then incubated for 24 hours at 37°C, after which dilutions of the mixture were plated onto TSB plates for CFU enumeration.

Single-cell RNA-seq

Pooled dorsal skin tissues from SA- or mock-infected mice (*n* = 3 animals per condition) were collected from vehicle or restraint-stressed mice 2 days postinfection. Tissues were minced, and single cells were isolated as previously described with minor modifications. Dead cells were removed using the Dead Cell Removal kit (Miltenyi Biotec, 130-090-101) following the manufacturer's instructions. Live cells were manually counted using a hemocytometer and resuspended in 0.04% Ultrapure bovine serum albumin (Thermo Fisher Scientific, AM2618) at a concentration of 1000 cells/μl. Gel bead-in-emulsion

(GEM) generation, barcoding, post-GEM-RT cleanup, cDNA amplification, and cDNA library construction were performed using Single Cell 3' v3 chemistry (10X Genomics). The cDNA libraries were sequenced on an Illumina HiSeq4000 platform (Illumina) [one lane, 100 PE (paired-end)]. Cell suspension, GEM generation, barcoding, post-GEM-RT cleanup, cDNA amplification, library preparation, quality control, and sequencing were conducted at the UCSD 10X Genomics Center. Quality control filtering was performed, applying the same metrics to all datasets. Cells were retained if they met the following criteria collectively: >200 genes per cell, <5000 genes per cell, <20% mitochondrial gene expression, <10% red cell gene expression, and < 40% ribosome gene expression. Low-quality cells and outliers were discarded, and only “valid” cells were used for downstream analyses.

Data integration, cell-cycle discrimination analyses, and agglomerative hierarchical clustering for scRNA-seq

We conducted data integration using the Seurat package (RStudio version 5.0.1). Integration anchors between datasets were identified using the FindIntegrationAnchors function (dims = 50) and integrated using the IntegrateData function (dims = 50). The integrated data were then scaled, and PCA was performed on highly variable features. Significant PCs were identified using a combination of statistical and heuristic methods and were used to guide clustering. Neighbors and clusters were identified using the FindNeighbors and FindClusters functions, respectively, and visualized using Uniform Manifold Approximation and Projection (UMAP) or tSNE. Cluster biomarkers were identified using the FindAllMarkers function (Wilcoxon rank-sum test). Scored cells were projected onto UMAP, and cells were color coded on the basis of their score. Cells present in each cell cycle phase were also quantified.

CellChat analysis

The R package CellChat was used to quantitatively infer and analyze intercellular communication networks on the basis of our scRNA-seq data. CellChat uses network analysis and pattern recognition methodologies to predict major signaling inputs and outputs for cells, as well as how these cells and signals coordinate for various functions. One of the key functionalities of CellChat is its ability to classify signaling pathways and delineate conserved and context-specific pathways through manifold learning and quantitative contrasts. Specifically, CellChat calculates the communication probability of a ligand-receptor pair between two cell types using a law of mass action model. This calculation considers factors such as ligand and receptor concentrations, known cofactor concentrations, and the number of cells in each cell type. To assess the significance of communication between two cell types, CellChat compares the communication probability of a ligand-receptor pair between these known cell types with the communication probability observed between randomly permuted groups of cells. If the communication probability is statistically higher between the known cell types compared with the permuted groups, then it indicates significant intercellular communication.

Oil Red O staining and quantification

An Oil Red O (Sigma-Aldrich, O0625) stock solution was prepared at a concentration of 3 mg/ml in 100% isopropanol. After stimulation, cells were washed three times with PBS and fixed in 10% formalin for 2 hours at room temperature. Subsequently, cells were rinsed with 60% isopropanol. Oil Red O working solution (diluted to 60% in dH₂O) was

then applied to cells for 2 hours and 30 min. Afterward, cells were rinsed again three times with PBS. For Oil Red O quantification, 500 µl of 100% isopropanol per well of a 24-well plate was added for 5 min and then removed, and absorbance at 492 nm was measured.

Bulk RNA-seq

HPAd and mouse dermal fibroblast cells were treated with adipocyte differentiation medium in the presence or absence of adrenaline, or mice skin biopsy samples were collected in triplicate. RNA was isolated from these samples and submitted to the UCSD Institute for Genomic Medicine (IGM) Center for RNA-seq analysis. The RNA-seq was conducted on a high-output run V4 platform (Illumina, USA) with single-read 100-cycle runs. During the analysis, the reads were aligned to the human reference genome (hg38) or the mouse reference genome (Ensembl release 102) using STAR. Subsequently, a counts table was generated using featureCounts. Normalization and differential expression analysis were then performed using DESeq2.

Lipidomic analysis

Lipidomic analysis was carried out at UCLA's Lipidomics Core using a standardized approach (90). Frozen skin tissue samples (50 to 100 mg) were first homogenized in PBS with ceramic beads using a bead-based homogenizer, applying three 10-s cycles. A portion of the homogenized tissue (3 to 6 mg) was then subjected to lipid extraction via a modified Bligh and Dyer method, with the addition of 70 internal lipid standards (from AB Sciex and Avanti) for quality assurance. The extracted lipids underwent two rounds of organic solvent extraction, after which the combined solvent layers were evaporated using a vacuum system (35°C, 90 min in total). The dried lipids were reconstituted in a methanol/dichloromethane mixture containing ammonium acetate and transferred to specialized vials for analysis. Lipid species were quantified using a Sciex 5500 instrument equipped with a differential mobility device (Lipidlyzer), calibrated with EquiSPLASH standards. The system detected more than 1450 lipid species across 17 subclasses using a predefined method. Data were processed via an in-house platform and normalized to tissue weight (milligram) to ensure accuracy.

Lesion size measurement in SA infection model

Total lesion size (mm²) was measured in the SA infection model by analyzing digital photographs with ImageJ software, calibrated against a millimeter ruler as the reference scale.

In vivo treatment with fingolimod (FTY720)

Fingolimod (FTY720, Cayman Chemical, 10006292) was prepared in a solution of 5% dimethyl sulfoxide; 40% polyethylene glycol, molecular weight 300; and 5% Tween 80. C57BL/6 mice received daily intraperitoneal injections of 100 µl of FTY720 at a dose of 3 mg/kg before the stress procedure, administered over a total of 4 days.

TGFβ administration

Recombinant mouse TGFβ1 (BioLegend, 763104) was administered via intradermal injection at a dose of 2 µg per mouse daily for a total of 3 days.

Epicutaneous and hindpaw SA infection model

A previously established mouse model of epicutaneous SA infection model was used (91). In general, the dorsal skin of each mouse was shaved and depilated using Nair cream. A 2 cm-by-2 cm sterile gauze pad was saturated with 100 µl of PBS containing 3×10^7 CFU

of USA300 and placed on the prepared skin, then covered with a transparent bio-occlusive dressing (Tegaderm; 3M) and secured with two layers of adhesive bandages (BAND-AID, Johnson & Johnson). After 24 hours, the gauze was removed, and skin biopsies were collected the following day. To induce hind paw infections, each hind-paw was injected subcutaneously with 5×10^6 CFU of USA300 in 20 μ l of PBS using a 0.5-cm³ syringe equipped with a 31-gauge needle (BD Biosciences).

Bacterial RNA extraction

USA300 was cultured in TSB with or without varying concentrations of stress hormones (0.1, 1, and 10 μ M) for 24 hours. After incubation, bacterial RNA was extracted using the Quick-RNA Fungal/Bacterial Miniprep kit (Zymo Research, R2014) according to the manufacturer's instructions.

Measurement of cell cytotoxicity with USA300 supernatant

USA300 was cultured in TSB, both with and without different concentrations of stress hormones (0.1, 1, and 10 μ M) for 24 hours. After this, a 10% USA300 supernatant was incubated with 8000 HaCaT cells for an additional 24 hours. Cell cytotoxicity was measured using the CyQUANT LDH cytotoxicity assay (Thermo Fisher Scientific, C20300) according to the manufacturer's protocol.

Protein immunoblot method

Total protein was extracted from cell pellets or skin tissues and separated on Novex Tricine protein gels (10 to 20%; Thermo Fisher Scientific, EC66252BOX). The proteins were then transferred onto polyvinylidene difluoride membranes using the Trans-Blot Turbo transfer pack (Bio-Rad, 1704156) and Trans-Blot Turbo transfer system (Bio-Rad, 1704150EDU). Membranes were blocked with Intercept (PBS) blocking buffer (LI-COR, 927-70001) for 2 hours at room temperature and subsequently incubated overnight at 4°C with primary antibodies against CRAMP (1:500; in house) or β -actin (1:2000; Cell Signaling Technology, 4967S). The following day, membranes were incubated with a secondary antibody (LI-COR, 926-68073) for 1 hour at room temperature. Protein bands were visualized using the Odyssey Classic Imager (LI-COR).

Statistical analysis

Statistical analyses were performed with GraphPad Prism 9 using unpaired two-tailed Student's *t* tests, Kruskal-Wallis test, or one-way analysis of variance (ANOVA). Multiple comparisons were adjusted using the Tukey's correction. Adjusted *P* values less than 0.05 were considered statistically significant. Details of all statistical tests are provided in the figure legends.

Supplementary Materials

The PDF file includes:

Figs. S1 to S16

Table S1

Other Supplementary Material for this manuscript includes the following:

Data files S1 and S2

MDAR Reproducibility Checklist

REFERENCES AND NOTES

- N. Barsotti, M. Chiera, D. Lanaro, M. Fioranelli, Impact of stress, immunity, and signals from endocrine and nervous system on fascia. *Front. Biosci.* **13**, 1–36 (2021).
- I.-G. Rojas, D. A. Padgett, J. F. Sheridan, P. T. Marucha, Stress-induced susceptibility to bacterial infection during cutaneous wound healing. *Brain Behav. Immun.* **16**, 74–84 (2002).
- J. P. Herman, J. M. McIlveen, S. Ghosal, B. Kopp, A. Wulsin, R. Makinson, J. Scheimann, B. Myers, Regulation of the hypothalamic-pituitary-adrenocortical stress response. *Compr. Physiol.* **6**, 603–621 (2016).
- S. A. Lowrance, A. Ionadi, E. McKay, X. Douglas, J. D. Johnson, Sympathetic nervous system contributes to enhanced corticosterone levels following chronic stress. *Psychoneuroendocrinology* **68**, 163–170 (2016).
- D. R. Seals, M. D. Esler, Human ageing and the sympathoadrenal system. *J. Physiol.* **528**, 407–417 (2000).
- F. S. Dhabhar, Enhancing versus suppressive effects of stress on immune function: Implications for immunoprotection and immunopathology. *Neuroimmunomodulation* **16**, 300–317 (2009).
- J. N. Morey, I. A. Boggero, A. B. Scott, S. C. Segerstrom, Current directions in stress and human immune function. *Curr. Opin. Psychol.* **5**, 13–17 (2015).
- J. S. Bains, K. A. Sharkey, Stress and immunity - the circuit makes the difference. *Nat. Immunol.* **23**, 1137–1139 (2022).
- A.-M. Globig, S. Zhao, J. Roginsky, V. I. Maltez, J. Guiza, N. Avina-Ochoa, M. Heeg, F. A. Hoffmann, O. Chaudhary, J. Wang, G. Senturk, D. Chen, C. O'Connor, S. Pfaff, R. N. Germain, K. A. Schalper, B. Emu, S. M. Kaech, The β_1 -adrenergic receptor links sympathetic nerves to T cell exhaustion. *Nature* **622**, 383–392 (2023).
- Y. Lai, R. L. Gallo, AMPD up immunity: How antimicrobial peptides have multiple roles in immune defense. *Trends Immunol.* **30**, 131–141 (2009).
- L.-J. Zhang, C. F. Guerrero-Juarez, T. Hata, S. P. Bapat, R. Ramos, M. V. Plikus, R. L. Gallo, Innate immunity. Dermal adipocytes protect against invasive *Staphylococcus aureus* skin infection. *Science* **347**, 67–71 (2015).
- L.-J. Zhang, S. X. Chen, C. F. Guerrero-Juarez, F. Li, Y. Tong, Y. Liang, M. Liggins, X. Chen, H. Chen, M. Li, T. Hata, Y. Zheng, M. V. Plikus, R. L. Gallo, Age-related loss of innate immune antimicrobial function of dermal fat is mediated by transforming growth factor beta. *Immunity* **50**, 121–136.e5 (2019).
- L.-J. Zhang, C. F. Guerrero-Juarez, S. X. Chen, X. Zhang, M. Yin, F. Li, S. Wu, J. Chen, M. Li, Y. Liu, S. I. B. Jiang, T. Hata, M. V. Plikus, R. L. Gallo, Diet-induced obesity promotes infection by impairment of the innate antimicrobial defense function of dermal adipocyte progenitors. *Sci. Transl. Med.* **13**, eabb5280 (2021).
- A. C. Campos, M. V. Fogaca, D. C. Aguiar, F. S. Guimaraes, Animal models of anxiety disorders and stress. *Braz. J. Psychiatry* **35**, S101–S111 (2013).
- K. M. Schneider, N. Blank, Y. Alvarez, K. Thum, P. Lundgren, L. Litichevskiy, M. Sleeman, K. Bahnsen, J. Kim, S. Kardo, S. Patel, L. Dohnalová, G. T. Uhr, H. C. Descamps, S. Kircher, A. M. McSween, A. R. Ardabili, K. M. Nemec, M. T. Jimenez, L. G. Glotfelty, J. D. Eisenberg, E. E. Furth, J. Henao-Mejia, F. C. Bennett, M. J. Pierik, M. Romberg-Camps, Z. Mujagic, M. Prinz, C. V. Schneider, E. J. Wherry, M. Bewtra, R. O. Heuckeroth, M. Levy, C. A. Thaiss, The enteric nervous system relays psychological stress to intestinal inflammation. *Cell* **186**, 2823–2838.e20 (2023).
- B. Zhang, S. Ma, I. Rachmin, M. He, P. Baral, S. Choi, W. A. Goncalves, Y. Schwartz, E. M. Fast, Y. Su, L. I. Zon, A. Regev, J. D. Buenrostro, T. M. Cunha, I. M. Chiu, D. E. Fisher, Y.-C. Hsu, Hyperactivation of sympathetic nerves drives depletion of melanocyte stem cells. *Nature* **577**, 676–681 (2020).
- G. R. Breese, T. D. Traylor, Effect of 6-hydroxydopamine on brain norepinephrine and dopamine: Evidence for selective degeneration of catecholamine neurons. *J. Pharmacol. Exp. Ther.* **174**, 413–420 (1970).
- N. J. Uretsky, L. L. Iversen, Effects of 6-hydroxydopamine on noradrenaline-containing neurones in the rat brain. *Nature* **221**, 557–559 (1969).
- J. M. Reel, J. Abbadi, A. J. Bueno, K. Cizio, R. Pippin, D. A. Doyle, L. Mortan, J. L. Bose, M. A. Cox, The sympathetic nervous system is necessary for development of CD4⁺ T-cell memory following *Staphylococcus aureus* Infection. *J. Infect. Dis.* **228**, 966–974 (2023).
- Y. R. Lankadeva, C. N. May, M. J. McKinley, M. R. Neeland, S. Ma, D. M. Hocking, R. Robins-Brown, S. Bedouli, D. G. S. Farmer, S. R. Bailey, D. Martelli, R. M. McAllen, Sympathetic nerves control bacterial clearance. *Sci. Rep.* **10**, 15009 (2020).
- S. Liu, C. Trapnell, Single-cell transcriptome sequencing: Recent advances and remaining challenges. *F1000Res* **5**, 182 (2016).
- T. Dokoshi, L.-J. Zhang, T. Nakatsuji, C. A. Adase, J. A. Sanford, R. D. Paladini, H. Tanaka, M. Fujiya, R. L. Gallo, Hyaluronidase inhibits reactive adipogenesis and inflammation of colon and skin. *JCI Insight* **3**, e123072 (2018).
- M. C. Liggins, F. Li, L.-J. Zhang, T. Dokoshi, R. L. Gallo, Retinoids enhance the expression of cathelicidin antimicrobial peptide during reactive dermal adipogenesis. *J. Immunol.* **203**, 1589–1597 (2019).
- H. Li, J. Niu, X. Wang, M. Niu, C. Liao, The contribution of antimicrobial peptides to immune cell function: A review of recent advances. *Pharmaceutics* **15**, 2278 (2023).
- C. Wagner, D. Kotsougianni, M. Pioch, B. Prior, A. Wentzensen, G. M. Hansch, T lymphocytes in acute bacterial infection: Increased prevalence of CD11b⁺ cells in the peripheral blood and recruitment to the infected site. *Immunology* **125**, 503–509 (2008).

26. D. Song, H. Jiao, Z. Liu, Phospholipid translocation captured in a bifunctional membrane protein Mprf. *Nat. Commun.* **12**, 2927 (2021).
27. C. M. Ernst, C. J. Slavetinsky, S. Kuhn, J. N. Hauser, M. Nega, N. N. Mishra, C. Gekeler, A. S. Bayer, A. Peschel, Gain-of-function mutations in the phospholipid flippase Mprf confer specific daptomycin resistance. *mBio* **9**, e0165918 (2018).
28. S. Jin, C. F. Guerrero-Juarez, L. Zhang, I. Chang, R. Ramos, C.-H. Kuan, P. Myung, M. V. Plukas, Q. Nie, Inference and analysis of cell-cell communication using CellChat. *Nat. Commun.* **12**, 1088 (2021).
29. J. Boucher, S. Softic, A. El Ouamari, M. T. Krumpoch, A. Kleinridders, R. N. Kulkarni, B. T. O'Neill, C. R. Kahn, Differential roles of insulin and IGF-1 receptors in adipose tissue development and function. *Diabetes* **65**, 2201–2213 (2016).
30. L. Hu, G. Yang, D. Hagg, G. Sun, J. M. Ahn, N. Jiang, C. L. Ricupero, J. Wu, C. H. Rodhe, J. A. Ascherman, L. Chen, J. J. Mao, IGF1 promotes adipogenesis by a lineage bias of endogenous adipose stem/progenitor cells. *Stem Cells* **33**, 2483–2495 (2015).
31. H. J. Lee, J. Lee, M. J. Yang, Y.-C. Kim, S. P. Hong, J. M. Kim, G.-S. Hwang, G. Y. Koh, Endothelial cell-derived stem cell factor promotes lipid accumulation through c-Kit-mediated increase of lipogenic enzymes in brown adipocytes. *Nat. Commun.* **14**, 2754 (2023).
32. K. Eismayr, A. Bestehorn, L. Morelli, M. Borroni, L. Vande Walle, M. Lamkanfi, P. Kovarik, Nonredundancy of IL-1 α and IL-1 β is defined by distinct regulation of tissues orchestrating resistance versus tolerance to infection. *Sci. Adv.* **8**, eabj7293 (2022).
33. L. S. Miller, E. M. Pietras, L. H. Uricchio, K. Hirano, S. Rao, H. Lin, R. M. O'Connell, Y. Iwakura, A. L. Cheung, G. Cheng, R. L. Modlin, Inflammasome-mediated production of IL-1 β is required for neutrophil recruitment against *Staphylococcus aureus* in vivo. *J. Immunol.* **179**, 6933–6942 (2007).
34. I. Kramerova, C. Kumagai-Cresse, N. Ermolova, E. Mokhovova, M. Marinov, J. Capote, D. Becerra, M. Quattrocelli, R. H. Crosbie, E. Welch, E. M. McNally, M. J. Spencer, Spp1 (osteopontin) promotes TGF β processing in fibroblasts of dystrophin-deficient muscles through matrix metalloproteinases. *Hum. Mol. Genet.* **28**, 3431–3442 (2019).
35. M. Kumar, D. Y. Makonchuk, H. Li, A. Mittal, A. Kumar, TNF-like weak inducer of apoptosis (TWEAK) activates proinflammatory signaling pathways and gene expression through the activation of TGF- β -activated kinase 1. *J. Immunol.* **182**, 2439–2448 (2009).
36. M. V. Guerin, F. Regnier, V. Feuillet, L. Vimeux, J. M. Weiss, G. Bismuth, G. Altan-Bonnet, T. Guilbert, M. Thoreau, V. Finisguerra, E. Donnadieu, A. Trautmann, N. Bercovici, TGF β blocks IFN α/β release and tumor rejection in spontaneous mammary tumors. *Nat. Commun.* **10**, 4131 (2019).
37. F. V. Castelino, G. Bain, V. A. Pace, K. E. Black, L. George, C. K. Probst, L. Goulet, R. Lafyatis, A. M. Tager, An autotaxin/lysophosphatidic acid/interleukin-6 amplification loop drives scleroderma fibrosis. *Arthritis Rheumatol.* **68**, 2964–2974 (2016).
38. K.-I. Jeon, K. Nehrke, K. R. Huxlin, Semaphorin 3A potentiates the profibrotic effects of transforming growth factor- β 1 in the cornea. *Biochem. Biophys. Res. Commun.* **521**, 333–339 (2020).
39. Z. Zhu, L. Guo, N. Yeltai, H. Xu, Y. Zhang, Chemokine (C-C motif) ligand 2-enhanced adipogenesis and angiogenesis of human adipose-derived stem cell and human umbilical vein endothelial cell co-culture system in adipose tissue engineering. *J. Tissue Eng. Regen. Med.* **16**, 163–176 (2022).
40. C. Li, J. Li, F. He, K. Li, X. Li, Y. Zhang, Matrix Gla protein regulates adipogenesis and is serum marker of visceral adiposity. *Adipocyte* **9**, 68–76 (2020).
41. K. Fujimori, M. Yano, T. Ueno, Synergistic suppression of early phase of adipogenesis by microsomal PGE synthase-1 (PTGES1)-produced PGE $_2$ and aldo-keto reductase 1B3-produced PGF $_{2\alpha}$. *PLOS ONE* **7**, e44698 (2012).
42. M. Chen, S. Kim, L. Li, S. Chattopadhyay, T. A. Rando, B. J. Feldman, Identification of an adipose tissue-resident pro-preadipocyte population. *Cell Rep.* **42**, 112440 (2023).
43. A. D. Hildreth, F. Ma, Y. Y. Wong, R. Sun, M. Pellegrini, T. E. O'Sullivan, Single-cell sequencing of human white adipose tissue identifies new cell states in health and obesity. *Nat. Immunol.* **22**, 639–653 (2021).
44. K. L. Whytock, Y. Sun, A. Divoux, G. Yu, S. R. Smith, M. J. Walsh, L. M. Sparks, Single cell full-length transcriptome of human subcutaneous adipose tissue reveals unique and heterogeneous cell populations. *iScience* **25**, 104772 (2022).
45. C. S. Smillie, M. Biton, J. Ordovas-Montanes, K. M. Sullivan, G. Burgin, D. B. Graham, R. H. Herbst, N. Rogel, M. Slyper, J. Waldman, M. Sud, E. Andrews, G. Velonias, A. L. Haber, K. Jagadeesh, S. Vickovic, J. Yao, C. Stevens, D. Dionne, L. T. Nguyen, A.-C. Villani, M. Hofree, E. A. Creasey, H. Huang, O. Rozenblatt-Rosen, J. J. Garber, H. Khalili, A. N. Desch, M. J. Daly, A. N. Ananthakrishnan, A. K. Shalek, R. J. Xavier, A. Regev, Intra- and inter-cellular rewiring of the human colon during ulcerative colitis. *Cell* **178**, 714–730.e22 (2019).
46. K. Pelka, M. Hofree, J. H. Chen, S. Sarkizova, J. D. Pirl, V. Jorgji, A. Bejnood, D. Dionne, W. H. Ge, K. H. Xu, S. X. Chao, D. R. Zollinger, D. J. Lieb, J. W. Reeves, C. A. Fuhrman, M. L. Hoang, T. Deloire, L. T. Nguyen, J. Waldman, M. Klapholz, I. Wakiro, O. Cohen, J. Albers, C. S. Smillie, M. S. Cuoco, J. Wu, M.-J. Su, J. Yeung, B. Vijaykumar, A. M. Magnuson, N. Asinovski, T. Moll, M. N. Goder-Reiser, A. S. Applebaum, L. K. Brais, L. K. Dello Stritto, S. L. Denning, S. T. Phillips, E. K. Hill, J. K. Meehan, D. T. Frederick, T. Sharova, A. Kanodia, E. Z. Todres, J. Jané-Vilbuena, M. Biton, B. Izar, C. D. Lambden, T. E. Clancy, R. Bleday, N. Melnitchouk, J. Irani, H. Kunitake, D. L. Berger, A. Srivastava, J. L. Hornick, S. Ogino, A. Rotem, S. Vigneau, B. E. Johnson, R. B. Corcoran, A. H. Sharpe, V. K. Kuchroo, K. Ng, M. Giannakis, L. T. Nieman, G. M. Boland, A. J. Aguirre, A. C. Anderson, O. Rozenblatt-Rosen, A. Regev, N. Hacohen, Spatially organized multicellular immune hubs in human colorectal cancer. *Cell* **184**, 4734–4752.e20 (2021).
47. S. Penuelas, J. Anido, R. M. Prieto-Sánchez, G. Folch, I. Barba, I. Cuartas, D. Garcia-Dorado, M. A. Poca, J. Sahúquillo, J. Baselga, J. Seoane, TGF- β increases glioma-initiating cell self-renewal through the induction of LIF in human glioblastoma. *Cancer Cell* **15**, 315–327 (2009).
48. C. Sacchetti, Y. Bai, S. M. Stanford, P. D. Benedetto, P. Cipriani, E. Santelli, S. Piera-Velazquez, V. Chernitskiy, W. B. Kiosses, A. Ceponis, K. H. Kaestner, F. Boin, S. A. Jimenez, R. Giacomelli, Z.-Y. Zhang, N. Bottini, PTP4A1 promotes TGF β signaling and fibrosis in systemic sclerosis. *Nat. Commun.* **8**, 1060 (2017).
49. Y. Yu, W. Wang, W. Lu, W. Chen, A. Shang, Inhibin β -A (INHBA) induces epithelial-mesenchymal transition and accelerates the motility of breast cancer cells by activating the TGF- β signaling pathway. *Bioengineered* **12**, 4681–4696 (2021).
50. H. Song, K. Fall, F. Fang, H. Erlendsdottir, D. Lu, D. Mataix-Cols, L. Fernandez de la Cruz, B. M. D'Onofrio, P. Lichtenstein, M. Gottfreðsson, C. Almqvist, U. A. Valdimarsdóttir, Stress related disorders and subsequent risk of life threatening infections: Population based sibling controlled cohort study. *BMJ* **367**, l5784 (2019).
51. G. A. Bin Saif, H. M. Alotaibi, A. A. Alzlobiani, N. A. Almodihesh, H. F. Albraidi, N. M. Alotaibi, G. Yosipovitch, Association of psychological stress with skin symptoms among medical students. *Saudi Med. J.* **39**, 59–66 (2018).
52. A. Yoshimura, Y. Wakabayashi, T. Mori, Cellular and molecular basis for the regulation of inflammation by TGF- β . *J. Biochem.* **147**, 781–792 (2010).
53. L. E. Hein, S. SenGupta, G. Gunasekaran, C. N. Johnson, C. A. Parent, TGF- β 1 activates neutrophil signaling and gene expression but not migration. *PLOS ONE* **18**, e0290886 (2023).
54. J. Reibman, S. Meixler, T. C. Lee, L. I. Gold, B. N. Cronstein, K. A. Haines, S. L. Kolasinski, G. Weissmann, Transforming growth factor beta 1, a potent chemoattractant for human neutrophils, bypasses classic signal-transduction pathways. *Proc. Natl. Acad. Sci. U.S.A.* **88**, 6805–6809 (1991).
55. R. L. Gallo, L. V. Hooper, Epithelial antimicrobial defence of the skin and intestine. *Nat. Rev. Immunol.* **12**, 503–516 (2012).
56. F. S. Dhabhar, K. Viswanathan, Short-term stress experienced at time of immunization induces a long-lasting increase in immunologic memory. *Am. J. Physiol. Regul. Integr. Comp. Physiol.* **289**, R738–R744 (2005).
57. A. Scanzano, M. Cosentino, Adrenergic regulation of innate immunity: A review. *Front. Pharmacol.* **6**, 171 (2015).
58. J. Zhou, J. Yan, H. Liang, J. Jiang, Epinephrine enhances the response of macrophages under LPS stimulation. *Biomed. Res. Int.* **2014**, 254686 (2014).
59. B. G. Song, M. G. Lim, J. H. Bae, J. H. Hong, S.-G. Lee, S. H. Park, C.-I. Kang, Multiple opportunistic infections related to hypercortisololemia due to adrenocortical carcinoma: A case report. *Infect. Chemother.* **53**, 797–801 (2021).
60. D. J. Torpy, J. T. Ho, Value of free cortisol measurement in systemic infection. *Horm. Metab. Res.* **39**, 439–444 (2007).
61. K. M. Rigby, F. R. DeLeo, Neutrophils in innate host defense against *Staphylococcus aureus* infections. *Semin. Immunopathol.* **34**, 237–259 (2012).
62. W. C. Poller, J. Downey, A. A. Mooslehner, N. Khan, L. Li, C. T. Chan, C. S. McAlpine, C. Xu, F. Kahles, S. He, H. Janssen, J. E. Mindur, S. Singh, M. G. Kiss, L. Alonso-Herranz, Y. Iwamoto, R. H. Kohler, L. P. Wong, K. Chetal, S. J. Russo, R. I. Sadreyev, R. Weissleder, M. Nahrendorf, P. S. Frenette, M. Divangahi, F. K. Swirski, Brain motor and fear circuits regulate leukocytes during acute stress. *Nature* **607**, 578–584 (2022).
63. S. W. Cole, S. P. Mendoza, J. P. Capitanio, Social stress desensitizes lymphocytes to regulation by endogenous glucocorticoids: Insights from *in vivo* cell trafficking dynamics in rhesus macaques. *Psychosom. Med.* **71**, 591–597 (2009).
64. B. Lopez-Garcia, P. H. Lee, K. Yamasaki, R. L. Gallo, Anti-fungal activity of cathelicidins and their potential role in *Candida albicans* skin infection. *J. Invest. Dermatol.* **125**, 108–115 (2005).
65. V. Nizet, T. Ohtake, X. Lauth, J. Trowbridge, J. Rudisill, R. A. Dorschner, V. Pestonjamasp, J. Piraino, K. Huttner, R. L. Gallo, Innate antimicrobial peptide protects the skin from invasive bacterial infection. *Nature* **414**, 454–457 (2001).
66. R. A. Dorschner, B. Lopez-Garcia, J. Massie, C. Kim, R. L. Gallo, Innate immune defense of the nail unit by antimicrobial peptides. *J. Am. Acad. Dermatol.* **50**, 343–348 (2004).
67. A. M. O'Neill, M. C. Liggins, J. S. Seidman, T. H. Do, F. Li, K. J. Cavagnero, T. Dokoshi, J. Y. Cheng, F. Shafiq, T. R. Hata, J. E. Gudjonsson, R. L. Modlin, R. L. Gallo, Antimicrobial production by perifollicular dermal preadipocytes is essential to the pathophysiology of acne. *Sci. Transl. Med.* **14**, eab1478 (2022).
68. S. X. Chen, L.-J. Zhang, R. L. Gallo, Dermal white adipose tissue: A newly recognized layer of skin innate defense. *J. Invest. Dermatol.* **139**, 1002–1009 (2019).
69. K. A. Radek, P. M. Elias, L. Taupenot, S. K. Mahata, D. T. O'Connor, R. L. Gallo, Neuroendocrine nicotinic receptor activation increases susceptibility to bacterial

- infections by suppressing antimicrobial peptide production. *Cell Host Microbe* **7**, 277–289 (2010).
70. M. H. Al-Wadei, H. A. N. Al-Wadei, H. M. Schuller, Pancreatic cancer cells and normal pancreatic duct epithelial cells express an autocrine catecholamine loop that is activated by nicotinic acetylcholine receptors $\alpha 3$, $\alpha 5$, and $\alpha 7$. *Mol. Cancer Res.* **10**, 239–249 (2012).
 71. H. A. N. Al-Wadei, M. H. Al-Wadei, H. M. Schuller, Cooperative regulation of non-small cell lung carcinoma by nicotinic and beta-adrenergic receptors: A novel target for intervention. *PLOS ONE* **7**, e29915 (2012).
 72. S. Sanjabi, S. A. Oh, M. O. Li, Regulation of the immune response by TGF- β : From conception to autoimmunity and infection. *Cold Spring Harb. Perspect. Biol.* **9**, a022236 (2017).
 73. S. G. Reed, TGF- β in infections and infectious diseases. *Microbes Infect.* **1**, 1313–1325 (1999).
 74. L. Garidou, S. Heydari, S. Gossa, D. B. McGavern, Therapeutic blockade of transforming growth factor beta fails to promote clearance of a persistent viral infection. *J. Virol.* **86**, 7060–7071 (2012).
 75. J. Massague, TGF- β signalling in context. *Nat. Rev. Mol. Cell Biol.* **13**, 616–630 (2012).
 76. D. Yin, D. Tuthill, R. A. Mufson, Y. Shi, Chronic restraint stress promotes lymphocyte apoptosis by modulating CD95 expression. *J. Exp. Med.* **191**, 1423–1428 (2000).
 77. W. Chen, M. E. Frank, W. Jin, S. M. Wahl, TGF- β released by apoptotic T cells contributes to an immunosuppressive milieu. *Immunity* **14**, 715–725 (2001).
 78. Y. Akiyama-Uchida, N. Ashizawa, A. Ohtsuru, S. Seto, T. Tsukazaki, H. Kikuchi, S. Yamashita, K. Yano, Norepinephrine enhances fibrosis mediated by TGF- β in cardiac fibroblasts. *Hypertension* **40**, 148–154 (2002).
 79. V. Raje, K. W. Ahern, B. A. Martinez, N. L. Howell, V. Oenarto, M. E. Granade, J. W. Kim, S. Tundup, K. Bottermann, A. Godecke, S. R. Keller, A. Kadl, M. L. Bland, T. E. Harris, Adipocyte lipolysis drives acute stress-induced insulin resistance. *Sci. Rep.* **10**, 18166 (2020).
 80. J. Han, Q. Meng, L. Shen, G. Wu, Interleukin-6 induces fat loss in cancer cachexia by promoting white adipose tissue lipolysis and browning. *Lipids Health Dis.* **17**, 14 (2018).
 81. G. van Hall, A. Steensberg, M. Sacchetti, C. Fischer, C. Keller, P. Schjerling, N. Hiscock, K. Moller, B. Saltin, M. A. Febbraio, B. K. Pedersen, Interleukin-6 stimulates lipolysis and fat oxidation in humans. *J. Clin. Endocrinol. Metab.* **88**, 3005–3010 (2003).
 82. H. Qing, R. Desrouleaux, K. Israni-Winger, Y. S. Mineur, N. Fogelman, C. Zhang, S. Rashed, N. W. Palm, R. Sinha, M. R. Picciotto, R. J. Perry, A. Wang, Origin and function of stress-induced IL-6 in murine models. *Cell* **182**, 372–387.e14 (2020).
 83. E. Arvat, B. Maccagno, J. Ramunni, L. Di Vito, R. Giordano, L. Gianotti, F. Broglia, F. Camanni, E. Ghigo, The inhibitory effect of alprazolam, a benzodiazepine, overrides the stimulatory effect of metyrapone-induced lack of negative cortisol feedback on corticotroph secretion in humans. *J. Clin. Endocrinol. Metab.* **84**, 2611–2615 (1999).
 84. R. Li, K. Bernau, N. Sandbo, J. Gu, S. Preissl, X. Sun, *Pdgfra* marks a cellular lineage with distinct contributions to myofibroblasts in lung maturation and injury response. *eLife* **7**, e36865 (2018).
 85. M. O'Rourke, C. L. Cullen, L. Auderset, K. A. Pitman, D. Achatz, R. Gasperini, K. M. Young, Evaluating tissue-specific recombination in a *Pdgfralpha-CreER*^{T2} transgenic mouse line. *PLOS ONE* **11**, e0162858 (2016).
 86. N. A. Veniaminova, Y. Y. Jia, A. M. Hartigan, T. J. Huyge, S.-Y. Tsai, M. Grachtchouk, S. Nakagawa, A. A. Dlugosz, S. X. Atwood, S. Y. Wong, Distinct mechanisms for sebaceous gland self-renewal and regeneration provide durability in response to injury. *Cell Rep.* **42**, 113121 (2023).
 87. S. Choi, B. Zhang, S. Ma, M. Gonzalez-Celeiro, D. Stein, X. Jin, S. T. Kim, Y.-L. Kang, A. Besnard, A. Rezza, L. Grisanti, J. D. Buenrostro, M. Rendl, M. Nahrendorf, A. Sahay, Y.-C. Hsu, Corticosterone inhibits GAS6 to govern hair follicle stem-cell quiescence. *Nature* **592**, 428–432 (2021).
 88. A. F. Zuluaga, B. E. Salazar, C. A. Rodriguez, A. X. Zapata, M. Agudelo, O. Vesga, Neutropenia induced in outbred mice by a simplified low-dose cyclophosphamide regimen: Characterization and applicability to diverse experimental models of infectious diseases. *BMC Infect. Dis.* **6**, 55 (2006).
 89. H. Chan, Q. Li, X. Wang, W. Y. Liu, W. Hu, J. Zeng, C. Xie, T. N. Y. Kwong, I. H. T. Ho, X. Liu, H. Chen, J. Yu, H. Ko, R. C. Y. Chan, M. Ip, T. Gin, A. S. L. Cheng, L. Zhang, M. T. V. Chan, S. H. Wong, W. K. K. Wu, Vitamin D₃ and carbamazepine protect against *Clostridioides difficile* infection in mice by restoring macrophage lysosome acidification. *Autophagy* **18**, 2050–2067 (2022).
 90. W.-Y. Hsieh, Q. D. Zhou, A. G. York, K. J. Williams, P. O. Scumpia, E. B. Kronenberger, X. P. Hoi, B. Su, X. Chi, V. L. Bui, E. Khialeeva, A. Kaplan, Y. M. Son, A. S. Divakaruni, J. Sun, S. T. Smale, R. A. Flavell, S. J. Bensinger, Toll-like receptors induce signal-specific reprogramming of the macrophage lipidome. *Cell Metab.* **32**, 128–143.e5 (2020).
 91. Y. Nakamura, J. Oscherwitz, K. B. Cease, S. M. Chan, R. Munoz-Planillo, M. Hasegawa, A. E. Villaruz, G. Y. C. Cheung, M. J. McGavin, J. B. Travers, M. Otto, N. Inohara, G. Nunez, *Staphylococcus* δ -toxin induces allergic skin disease by activating mast cells. *Nature* **503**, 397–401 (2013).

Acknowledgments: All sequencing was performed at the IGM at UCSD. Graphical abstract and figure schematics were created with Biorender.com. **Funding:** R.L.G. is supported by NIH R37AI052453, R01DK128787, and P50AR080594. I.M.C. is supported by NIH R01AI168005. O.V. and W.C. are supported by the Intramural Research Program of NIH, NIDCR. **Author contributions:** The conceptualization of the study was carried out by H.C. and R.L.G. The methodology was developed by H.C., F.L., T.D., K.J.C., Q.L., and Y.C. The investigation involved H.C., F.L., C.A., T. Nakatsuji, E.L., A.I., D.Y., O.V., T. Numata, B.C., and H.L. Visualization was handled by K.J.W. and S.J.B. The original draft was written by H.C. and R.L.G., whereas the writing—review and editing were conducted by H.C., W.J.C., I.M.C., and R.L.G. **Competing interests:** R.L.G. is a cofounder, scientific advisor, consultant, and equity holder of MatriSys Biosciences. I.M.C. consults for GSK pharmaceuticals and Nilo Inc. **Data and materials availability:** All data needed to evaluate the conclusions in the paper are present in the paper or the Supplementary Materials. Sequencing data have been deposited under the accession numbers GSE270712 and GSE270713. All requests for resources and reagents should be directed to R.L.G. (rgallo@ucsd.edu) and will be fulfilled upon request.

Submitted 26 July 2024
Resubmitted 22 November 2024
Accepted 17 March 2025
Published 11 April 2025
10.1126/scimmunol.ads0519